

# Efficient Fast-Convolution Based Waveform Processing for 5G Physical Layer

Juha Yli-Kaakinen, Toni Levanen, Sami Valkonen, Kari Pajukoski, Juho Pirskanen,  
Markku Renfors, *Fellow, IEEE*, and Mikko Valkama, *Senior Member, IEEE*

**Abstract**—This paper investigates the application of fast-convolution (FC) filtering schemes for flexible and effective waveform generation and processing in 5th generation (5G) systems. FC based filtering is presented as a generic multimode waveform processing engine while, following the progress of 5G new radio (NR) standardization in 3rd Generation Partnership Project (3GPP), the main focus is on efficient generation and processing of subband-filtered cyclic prefix orthogonal frequency-division multiplexing (CP-OFDM) signals. First, a matrix model for analyzing FC filter processing responses is presented and used for designing optimized multiplexing of filtered groups of CP-OFDM physical resource blocks (PRBs) in a spectrally well-localized manner, i.e., with narrow guardbands. Subband filtering is able to suppress interference leakage between adjacent subbands, thus supporting independent waveform parametrization and different numerologies for different groups of PRBs, as well as asynchronous multiuser operation in uplink. These are central ingredients in the 5G waveform developments, particularly at sub-6 GHz bands. The FC filter optimization criterion is passband error vector magnitude minimization subject to a given subband band-limitation constraint. Optimized designs with different guardband widths, PRB group sizes, and essential design parameters are compared in terms of interference levels and implementation complexity. Finally, extensive coded 5G radio link simulation results are presented to compare the proposed approach with other subband-filtered CP-OFDM schemes and time-domain windowing methods, considering cases with different numerologies or asynchronous transmissions in adjacent subbands. Also the feasibility of using independent transmitter and receiver processing for CP-OFDM spectrum control is demonstrated.

**Index Terms**—5G, physical layer, 5G New Radio, 5G-NR, multicarrier, waveforms, filtered-OFDM, fast-convolution

## I. INTRODUCTION

**O**RTHOGONAL frequency-division multiplexing (OFDM) is extensively utilized in modern radio access systems. This is due to the high flexibility and

This work was partially supported by the Finnish Funding Agency for Technology and Innovation (Tekes) and Nokia Bell Labs, under the projects “Phoenix+”, “5G Radio Systems Research”, and “Wireless for Verticals (WIVE)”, and in part by the Academy of Finland under the project no. 284694 and no. 284724. Early stage results of this paper have been submitted to EUCNC 2017, Oulu, Finland [1]

Juha Yli-Kaakinen, Toni Levanen, Sami Valkonen, Markku Renfors, and Mikko Valkama are with the Department of Electronics and Communications Engineering, Tampere University of Technology, FI-33101 Tampere, Finland (e-mail: {juha.yli-kaakinen; toni.levanen; sami.valkonen; markku.renfors; mikko.e.valkama}@tut.fi)

Kari Pajukoski and Juho Pirskanen are with the Nokia Bell Labs, Finland (e-mail: {kari.pajukoski; juho.pirskanen}@nokia-bell-labs.com)

Digital Object Identifier 10.1109/JSAC.2017.2687358

efficiency in allocating spectral resources to different users, simple and robust way of channel equalization, as well as simplicity of combining multiantenna schemes with the core physical layer processing [2]. However, due to limited spectrum localization, OFDM has major limitations in challenging new spectrum use scenarios, like asynchronous multiple access, as well as mixed numerology cases aiming to use adjustable subcarrier spacing (SCS), symbol length, and cyclic prefix (CP) length, depending on the service requirements [3], [4].

The debate over different waveform candidates for the 5th generation new radio (5G-NR) physical layer has been exhaustive during the last few years. Researchers have revised their knowledge over different waveforms thoroughly, evaluating, e.g., filter bank based orthogonal and non-orthogonal multi-carrier waveforms [3], [4]. Regarding OFDM based advanced waveform candidates, subband-filtered CP-OFDM schemes are receiving great attention in the 5G waveform development, due to their ability to address the mentioned issues while maintaining high level of commonality with legacy OFDM systems. Generally, these schemes apply filtering at subband level, over a physical resource block group including single or multiple PRBs. In the existing studies, different window based time-domain filtering schemes have been considered in [5] (referred to as universal filtered OFDM (UF-OFDM)) and in [6] (referred to as filtered-OFDM (f-OFDM)). Effective uniform polyphase filter bank structures have been considered in [7] (referred to as RB-F-OFDM). In our recent study, flexible and effective frequency-domain filtering scheme, based on fast-convolution (FC), was proposed for filtered OFDM in [8] whereas the possibility to design parametrizations supporting adjustable CP lengths with fixed overall CP-OFDM symbol duration was demonstrated in [9]. FC based realization of UF-OFDM has also been proposed in [10]. We see these as alternative implementations of the same idea. While noting that subband-filtered zero-prefix OFDM variants have also been considered, 5G-NR development focuses on CP-OFDM and we refer to these schemes jointly as subband filtered CP-OFDM (F-OFDM) throughout this paper. As an alternative approach for enhancing the CP-OFDM spectrum, windowed overlap-and-add (WOLA) based CP-OFDM [11] is regarded as another strong 5G waveform candidate.

Less studies have been devoted to situations where the transmitter and receiver utilize different waveform processing techniques. The recent development in the specification of

5G-NR in 3GPP technical specification group (TSG)-radio access network (RAN) WG1 stated that the baseline assumption of the waveform for below 40 GHz communications is CP-OFDM and that the transmitter (TX) processing has to be transparent to the receiver (RX) [12], [13]. This means that the possible spectrum enhancement function performed in TX is not signaled to RX and it is generally an unknown, implementation dependent function. This implies that TX and RX waveform processing are typically not matched, and that they need to be evaluated separately. It is expected that F-OFDM or WOLA is applied on the TX side when improved spectrum localization is required, and the RX processing is selected without knowledge of the detailed transmission scheme.

In this paper, we develop and provide a generic and universal optimization-based framework for FC-based F-OFDM (FC-F-OFDM) waveform processing for 5G physical layer and evaluate its performance in scenarios following the test cases defined by 3GPP [14, Annex A]. More specifically, the main contributions of the present paper can be listed as follows:

- FC based frequency-domain windowing is shown to be an effective way to realize subband-filtered OFDM schemes, with significantly lower computational complexity and highly increased flexibility compared to time-domain filtering approaches.
- Analytical models are developed for the essential responses of FC based synthesis and analysis processing and for the resulting passband error vector magnitude (EVM) and subband leakage ratio (SBLR) performance.
- These models are used for effectively optimizing subband filtering with very narrow guardbands (1–7 subcarriers) between groups of PRBs. The optimization minimizes directly the distortion introduced by partial suppression of the sidelobes of the subcarriers close to the subband edges. The number of non-trivial frequency-domain windowing weights is minimized, resulting in substantially reduced processing complexity and memory requirements.
- Comprehensive coded 5G radio link simulations are carried out for evaluating the performance of FC-F-OFDM, based on tentative 3GPP 5G-NR numerology and test cases. Also comparisons with WOLA and other existing F-OFDM proposals are included.
- In general, these results demonstrate the good performance, flexibility, and efficiency of the proposed scheme with different sizes of PRB groups facilitating better radio link performance with lower complexity compared to other existing F-OFDM schemes.
- Fast-convolution filter bank (FC-FB) is presented (see Section II-C) as a generic waveform processing engine for evolving cellular mobile communications systems, supporting also, e.g., traditional single-carrier waveforms with frequency-domain equalization (considered in 5G for above-40 GHz frequency bands) in an effective and flexible manner.

In the proposed approach, frequency-domain windowing is defined by a very low number of weight coefficients, which facilitates efficient implementation and direct filter

optimization for specific EVM, SBLR and out-of-band (OOB) emission requirements. The widths and center frequencies can be adjusted individually for each subband, which is not possible in F-OFDM schemes based on traditional uniform filter bank approaches, like [7]. On the other hand, individual time-domain filtering, as proposed in [5], [6], becomes overly complicated to implement. Even in case of a single subband (e.g., channelization filtering for the whole carrier) FC filtering provides competitive performance vs. complexity tradeoffs. Time-domain windowing methods, like WOLA, exhibit excellent passband EVM performance but their spectrum localization capability, in terms of SBLR and OOB emissions, is rather limited compared to all F-OFDM schemes, unless the symbol duration is greatly extended to accommodate long window transition intervals.

The remainder of this paper is organized as follows. In Section II, the multirate FC idea and FC-FB concept are introduced, along with a basic matrix model for analysis and optimization purposes. This model was developed originally in [15] for filter bank multicarrier (FBMC) cases and is here specifically tailored for efficient F-OFDM processing and optimization. Also the use of FC-FB as a generic waveform processing engine is discussed. Section III develops analytical matrix models for evaluating the EVM and SBLR in the FC-F-OFDM systems. Then the FC-F-OFDM physical layer processing design is formulated as an optimization problem. In this problem the goal is to minimize the maximum of the subcarrier-level passband EVM subject to the given subband band-limitation constraint. Numerical results for the optimized scheme with tentative 3GPP 5G-NR numerology and with alternative design parameters are provided as well. In Section IV, extensive coded 5G radio link simulations are reported for evaluating the performance of FC based F-OFDM and DFT-spread-OFDM in various different test cases. Finally, the conclusions are drawn in Section V.

## II. MULTIRATE FAST-CONVOLUTION AND FILTER BANKS

The main idea of FC is that a high-order filter can be implemented effectively through multiplication in frequency domain, after taking discrete Fourier transforms (DFTs) of the input sequence and the filter impulse response. Then the time-domain output signal is obtained by inverse discrete Fourier transform (IDFT). In practice, efficient implementation techniques, like fast Fourier transform (FFT) and inverse fast Fourier transform (IFFT), are used for the transforms, and overlap-save processing is applied for long sequences [16].

The application of FC to multirate filters has been presented in [17], and FC implementations of channelization filters have been considered in [18], [19], [20]. The authors have introduced the idea of FC-implementation of nearly perfect-reconstruction filter bank systems and detailed analysis and FC-FB optimization methods are developed in [21]. In [22] FC approach has been applied for filter bank multicarrier waveforms and in [23] for flexible single-carrier (SC) waveforms. These papers demonstrate the flexibility and efficiency of FC-FB in communications signal processing, in general. In this article, the focus is fully on subband-filtered CP-OFDM.

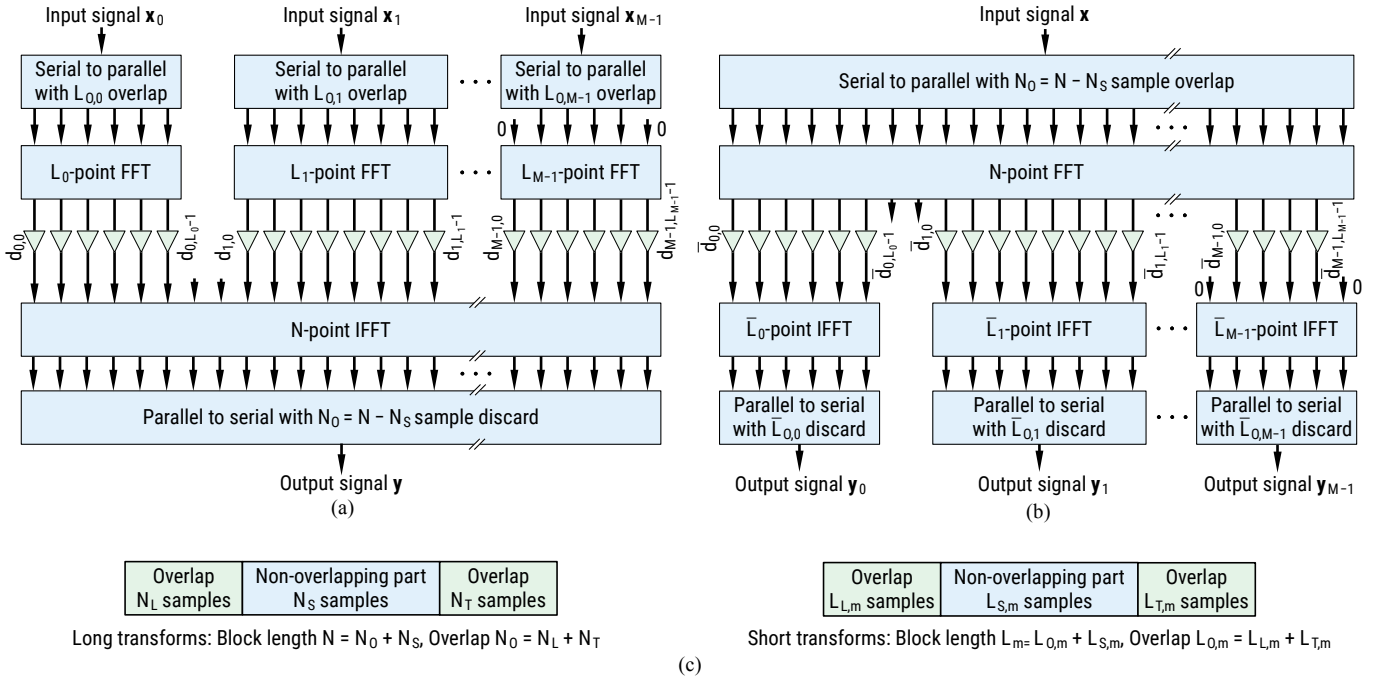


Fig. 1: (a) FC based flexible synthesis filter bank structure. (b) Corresponding FC analysis filter bank structure. (c) Notations used for the number of samples in different parts of the overlap-save blocks.

### A. Fast-Convolution Filter Bank Schemes

Fig. 1(a) shows the structure of FC-based flexible synthesis filter bank (SFB), for a case where the  $M$  incoming low-rate, narrowband signals  $x_m$  for  $m = 0, 1, \dots, M-1$  with adjustable frequency responses and adjustable sampling rates are to be combined into single wideband signal  $y$ . The dual structure shown in Fig. 1(b) can be used on the receiver side as an analysis filter bank (AFB) for splitting the incoming high-rate, wideband signal into several narrowband signals [24]. The cascade of SFB and AFB is often called transmultiplexer.

In the SFB case, each of the  $M$  incoming signals is first segmented into overlapping blocks of length  $L_m$ . Then, each input block is transformed to frequency-domain using DFT of length  $L_m$ . The frequency-domain bin values of each converted subband signal are multiplied by the weight values corresponding to the DFT of the finite-length linear filter impulse response,  $d_{\ell,m} = \sum_{n=0}^{L_m-1} h_m[n] e^{-j2\pi(\ell+L_m/2)n/L_m}$  for  $\ell = 0, 1, \dots, L_m-1$  and for  $m = 0, 1, \dots, M-1$ .<sup>1</sup> Here,  $\ell$  is the DFT bin index within the subband and  $m$  is the subband index. Finally, the weighted signals are combined and converted back to time-domain using IDFT of length  $N$  and the resulting time-domain output blocks are concatenated using the overlap-save principle [16], [25].

The multirate FC-processing of Fig. 1(a) increases the sampling rates of the subband signals by the factors of

$$I_m = N/L_m = N_S/L_{S,m}, \quad (1)$$

where  $L_{S,m}$  and  $N_S$  are the numbers of non-overlapping input and output samples, respectively. The number of overlapping

samples  $L_{0,m} = L_m - L_{S,m}$  is divided into leading and trailing overlapping parts as follows:

$$L_{L,m} = \lceil (L_m - L_{S,m})/2 \rceil \quad \text{and} \quad L_{T,m} = \lfloor (L_m - L_{S,m})/2 \rfloor. \quad (2)$$

Given the IDFT length  $N$ , the sampling rate conversion factor is determined by the DFT length  $L_m$ , and it can be configured for each subband individually. Generally, there is no need to restrict the sampling rate conversion factor to take integer values. Naturally,  $L_m$  determines the maximum number of non-zero frequency bins, i.e., the bandwidth of the subband.

We assume an FC-FB parametrization where the overlapping block structures at low-rate and high-rate sides match exactly, such that overlapping and non-overlapping parts can be expressed as an integer number of samples, corresponding to the same time duration on both sides. This is reached if  $N$ ,  $L$ ,  $N_S$ , and  $L_{S,m}$  take integer values in (1) for all subbands. Generally,  $N = p\Gamma$  and  $N_S = q\Gamma$ , where  $p$  and  $q$  are two relatively prime integers and  $\Gamma = \text{gcd}(N, N_S)$ , where  $\text{gcd}(\cdot)$  is the greatest common divisor. Then for the narrowest possible subband case satisfying the integer-length criterion,  $L_m = p$  and  $L_{S,m} = q$ . Generally,  $L_m$  has to be a multiple of  $N/\Gamma$ , that is, the configurability of the subband sampling rates depends greatly on the choice of  $N$  and  $N_S$ .

In the AFB case, it is assumed that the forward transform length is larger than the inverse transform lengths and, therefore, the above process reduces the sampling rate of the subband signal by factors of

$$D_m = N/\bar{L}_m = N_S/\bar{L}_{S,m}. \quad (3)$$

Here, the IDFT lengths on the AFB side are denoted by  $\bar{L}_m$ 's. For simplicity, it is assumed that the long transform length  $N$  for SFB and AFB is the same.

<sup>1</sup>For convenience of notation, we use the "FFT-shifted" indexing scheme in this context, i.e., index 0 corresponds to the lower edge of the subband.

In [21] and [24], the performance of the FC-FB was analyzed using a periodically time-variant model and tools for frequency response analysis and FC-FB optimization were developed. In the following sections, we first summarize the generic matrix model for FC-FB analysis, and then develop FC-FB analysis and optimization tools for the F-OFDM based 5G-NR physical layer.

### B. Matrix Model for FC-FB Analysis and Optimization

In the FC SFB case, the block processing of  $m$ th subband signal  $\mathbf{x}_m$  for the generation of high-rate subband waveform  $\mathbf{w}_m$  can be represented as

$$\mathbf{w}_m = \mathbf{F}_m \mathbf{x}_m, \quad (4a)$$

where  $\mathbf{F}_m$  is the block diagonal transform matrix of the form

$$\mathbf{F}_m = \text{diag}(\mathbf{F}_{m,0}, \mathbf{F}_{m,1}, \dots, \mathbf{F}_{m,R_m-1}) \quad (4b)$$

with  $R_m$  blocks. Here, the dimensions and locations of the  $\mathbf{F}_{m,r}$ 's are determined by the overlapping factor of the overlap-save processing, defined as

$$\lambda = 1 - L_{S,m}/L_m = 1 - N_S/N. \quad (5)$$

The multirate version of the FC SFB can be represented using block processing by decomposing the  $\mathbf{F}_{m,r}$ 's as the following  $N_S \times L_m$  matrix

$$\mathbf{F}_{m,r} = \mathbf{S}_N \mathbf{W}_N^{-1} \mathbf{M}_{m,r} \mathbf{D}_m \mathbf{P}_{L_m}^{(L_m/2)} \mathbf{W}_{L_m}. \quad (6)$$

Here,  $\mathbf{W}_{L_m}$  and  $\mathbf{W}_N^{-1}$  are the  $L_m \times L_m$  DFT matrix (with  $[\mathbf{W}_{L_m}]_{p,q} = e^{-j2\pi(p-1)(q-1)/L_m}$ ) and  $N \times N$  inverse DFT matrix, respectively. The DFT shift matrix  $\mathbf{P}_{L_m}^{(L_m/2)}$  is circulant permutation matrix obtained by cyclically left shifting the  $L_m \times L_m$  identity matrix by  $L_m/2$  positions.  $\mathbf{D}_m$  is the  $L_m \times L_m$  diagonal matrix with the frequency-domain window weights of the subband  $m$  on its diagonal. The  $N \times L_m$  frequency-domain mapping matrix  $\mathbf{M}_{m,r}$  maps  $L_m$  frequency-domain bins of the input signal to frequency-domain bins  $(c_m - \lceil L_m/2 \rceil + \ell)_N$  for  $\ell = 0, 1, \dots, L_m - 1$  of output signal. Here  $c_m$  is the center bin of the subband  $m$  and  $(\cdot)_N$  denotes the modulo- $N$  operation. In addition, this matrix rotates the phases of the block by

$$\theta_m(r) = \exp(j2\pi r \theta_m) \quad \text{with} \quad \theta_m = c_m L_{S,m}/L_m \quad (7)$$

in order to maintain the phase continuity between the consecutive overlapping processing blocks [21]. The  $N_S \times N$  selection matrix  $\mathbf{S}_N$  selects the desired  $N_S$  output samples from the inverse transformed signal corresponding to overlap-save processing. The FC SFB processing in the FC-F-OFDM context is illustrated later in Fig. 5.

In the AFB case, the corresponding analysis sub-block matrix of size  $\bar{L}_{S,m} \times N$  can be decomposed as

$$\mathbf{G}_{m,r} = \mathbf{S}_{L_m} \mathbf{W}_{L_m}^{-1} \mathbf{P}_N^{(N/2)} \mathbf{D}_m \mathbf{M}_{m,r}^T \mathbf{W}_N, \quad (8)$$

where  $\mathbf{P}_N^{(N/2)}$  is the  $N \times N$  inverse Fourier-shift matrix and the  $\bar{L}_{S,m} \times \bar{L}_m$  selection matrix  $\mathbf{S}_{L_m}$  selects the desired  $\bar{L}_{S,m}$  output samples from the inverse transformed output signal.

In general, the above FC based synthesis and analysis filter banks are linear periodically shift variant (LPSV) systems with

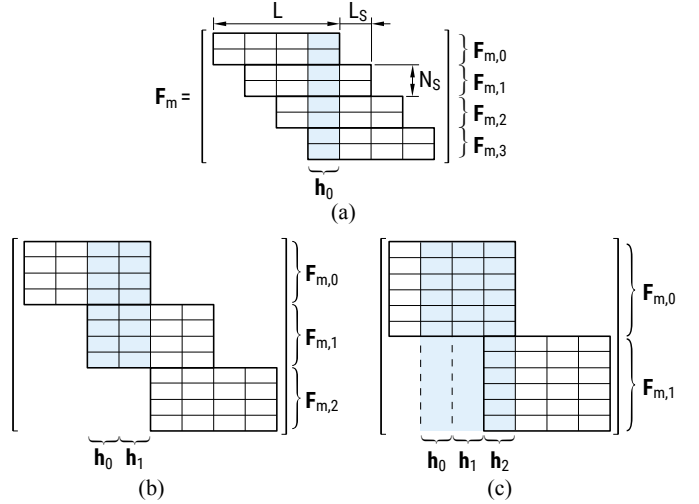


Fig. 2: Structure of block-diagonal synthesis matrix  $\mathbf{F}_m$  for  $L_m = 4$ ,  $N = 8$ , and  $L_{S,m} = 1, 2, 3$  ( $\lambda = 3/4, 2/4, 1/4$ ). The colored columns illustrate the elements of the synthesis matrix that form the shift-variant impulse responses of the synthesis filter bank. (a) For  $L_{S,m} = 1$ , the system has only one impulse response of eight samples. (b) For  $L_{S,m} = 2$ , the system has two eight-samples long responses. (c) For  $L_{S,m} = 3$ , two among the three responses are six samples long and the remaining one is 12 samples long.

period of  $L_{S,m}$ , that is, the systems have  $L_{S,m}$  different impulse responses. In the SFB case, the impulse responses are given by the  $L_{S,m}$  shift-variant columns of the  $\mathbf{F}_m$  as illustrated Fig. 2.

In our approach, FC design is done in frequency-domain by defining/optimizing the weight coefficients. Generally, the frequency-domain weights consist of two symmetric transition bands with  $L_{TBW,m}$  non-trivial weights, where  $L_{TBW,m}$  also defines the transition-band width (TBW) for subband  $m$ . All passband weights are set to one, and all stopband weights are set to zero. The number of stopband weights (and the corresponding transform length) can be selected to reach a feasible subband oversampling factor. Now the diagonal weighting matrix in (6) and (8) is expressible as

$$\mathbf{D}_m = \text{diag} \left( \begin{array}{c} \mathbf{0}_{(\lceil [L_m - L_{ACT,m}]/2 \rceil - L_{TBW,m}) \times 1} \\ d_{0,m} \\ \dots \\ d_{L_{TBW,m}-1,m} \\ \mathbf{1}_{L_{ACT,m} \times 1} \\ d_{L_{TBW,m}-1,m} \\ \dots \\ d_{0,m} \\ \mathbf{0}_{(\lceil [L_m - L_{ACT,m}]/2 \rceil - L_{TBW,m}) \times 1} \end{array} \right), \quad (9)$$

where  $L_{ACT,m}$  is the number of active subcarriers on subband  $m$ , and  $\mathbf{0}_{q \times 1}$  is the column vector of  $q$  zeros whereas  $\mathbf{1}_{p \times 1}$  is the vector of  $p$  ones. Fig. 3 shows the weights for two example cases with different bandwidths.

### C. FC-FB as a Generic Waveform Processing Engine

FC-FB was originally applied for channelization filtering [18], [19], [20], and it can be used for that purpose in a very flexible manner, allowing simultaneous transmission/reception of different waveforms with arbitrary bandwidths and channel rasters. After establishing the idea that FC-FB can be used for realizing nearly perfect-reconstruction filter bank systems



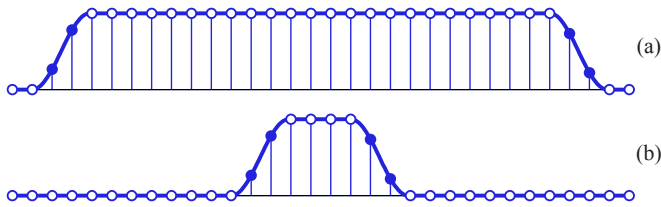


Fig. 3: Examples of FFT-domain weight masks. (a) Single subband with wider bandwidth. (b) Single subband with narrower bandwidth. The ( $L_{TBW} = 2$ ) non-trivial transition-band weights are denoted by filled circles.

[21], it was utilized for the generation and detection of filter bank multicarrier with offset-QAM subcarrier modulation (FBMC/OQAM) and filtered multitone (FMT) type multicarrier waveforms [22]. It was applied also for traditional Nyquist pulse shaping based SC waveforms, with adjustable and possibly very small roll-off [23]. Basically the same processing structure, but without overlap processing, can be used also for implementing circular multicarrier waveforms like generalized frequency-division multiplexing (GFDM) [3], and block-CP variants of FBMC/OQAM and FMT [26]. In the cellular mobile communication context the flexibility of FC-FB can be exploited, for example, in multi-standard broadband base-station transmitters and receivers for simultaneous channelization of GSM, WCDMA, long-term evolution (LTE) carriers, as well as subbands of PRB groups in 5G-NR.

Fig. 3 illustrates how different FC subband filters can be constructed using a fixed transition band weight mask. The subband frequency responses are constructed by adding one-valued weights between symmetric transition bands and zero-valued weights outside the transition bands. In this way the bandwidth, sampling rate conversion factor, and roll-off can be adjusted in a flexible manner. While the weights can be optimized separately for each case, the performance reduction is usually rather small when using a well-optimized fixed weight mask. This implies that the whole FC-FB can be stored to device memory only with  $L_{TBW}$  non-trivial transition band weights which are used with all different subband widths. In general, this is a remarkable implementation benefit.

The parametrization for a flexible FC-FB processing engine depends mainly on the needed spectral resolution: The narrowest transition bandwidth should be in the order of 2–7 FFT bin spacings, depending on the passband EVM and subband band limitation requirements. After fixing the FFT bin spacing, the long transform length follows directly from the targeted overall bandwidth.

Also synchronization and channel equalization functions can be integrated with the FFT-domain processing of FC-FB. Timing offsets in different subbands can be compensated by introducing a proper linearly frequency-dependent phase term in the weights [27]. Also a way to compensate fractional frequency offsets (with respect to the FFT bin spacing) has been presented in [28]. Channel equalization can be realized for different waveforms in a unified manner by combining the channel equalization weights with the subband weight masks [29]. However, in case of FC-F-OFDM, it is straightforward and computationally more effective to do the channel equalization in the traditional way in the RX OFDM processing

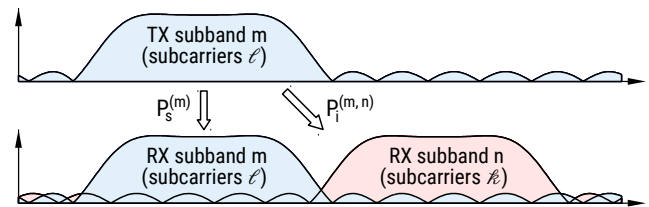


Fig. 4: Illustration of the subband leakage ratio evaluation.

module.

### III. FC-BASED F-OFDM FOR 5G PHYSICAL LAYER

#### A. FC-based F-OFDM

In FC-based F-OFDM (FC-F-OFDM), we apply FC-FB based filtering at subband level, which means one or multiple contiguous PRBs, while utilizing normal CP-OFDM waveform for the PRBs [8], [9]. One clear application is in cellular uplink scenarios, in which the different user equipments (UEs) utilize different sets of PRBs for their simultaneous transmissions. In such cases, an individual UE can adopt the subband filtering separately for each contiguous set of PRBs allocated to it. This, together with similar FC-based subband filtering at the base-station receiver, allow for reduced uplink timing synchronization requirements, or even completely asynchronous uplink, as well as enable adopting different numerologies (e.g., different subcarrier spacings, CP-lengths, and/or frame structures) [9], for different UEs and services simultaneously inside the carrier. Furthermore, if the allocated uplink (UL) PRBs are at the channel edge, subband filtering at the UE transmitter contributes to reducing the OOB emissions. Additionally, in dynamic time-division duplexing (TDD) networks with frequency reuse 1, better band-limitation of the uplink subband signals also helps in reducing the intercell interference between neighboring subbands.

Concerning the cellular downlink scenarios, synchronization is basically not an issue, but the filtered OFDM idea would still make it possible to parametrize individually the subsignals of different groups of PRBs, inside the carrier, and thus facilitate flexible multiplexing of UEs and services also in the downlink. Interestingly, in downlink CoMP type scenarios, this would also allow for tuning the downlink transmit signal timing in an individual transmission point, separately for different UEs at different subbands.

With FC-F-OFDM processing, it is easy to adjust the filtering bandwidth for the subbands individually. This is very useful in PRB-filtered OFDM because there is no need to realize filter transition bands and guardbands between equally parametrized, synchronous PRBs. In the extreme case, the group of filtered PRBs could cover the full carrier bandwidth, and FC processing would implement tight channelization filtering for the whole carrier. Fig. 5 shows a generic block diagram of a FC-F-OFDM transmitter. The FC's long transform length  $N$  is assumed to be fixed in the following discussions.

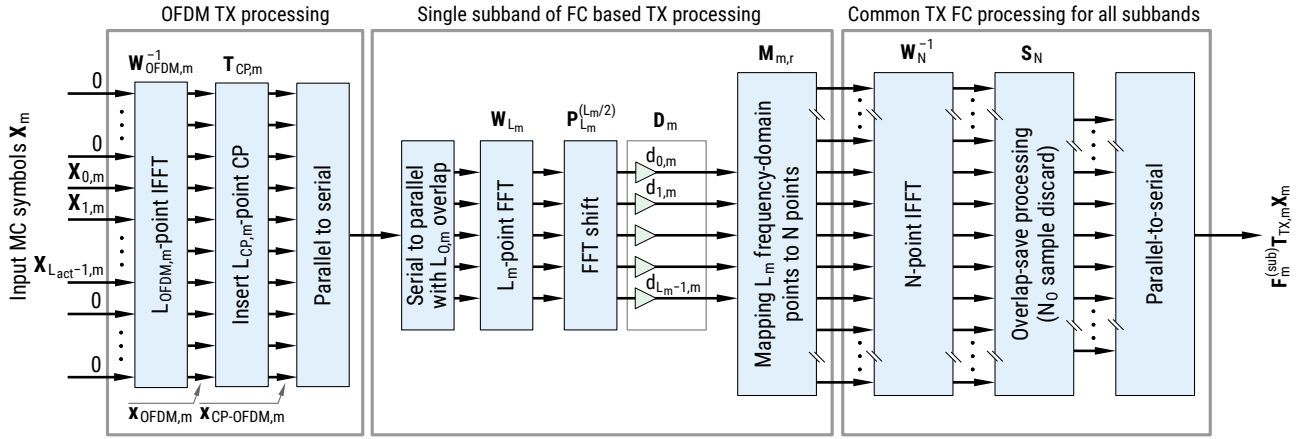


Fig. 5: FC-F-OFDM transmitter. The processing structure for one filtered group of PRBs is shown (cf. Fig. 1(a) for the overall synthesis processing). The long  $N$ -point IFFT is common for all the subbands.

### B. Transmultiplexer Optimization for FC-F-OFDM

The CP-OFDM processing of the  $m$ th OFDM subband on the transmitter side can be expressed as

$$\mathbf{T}_{TX,m} = \mathbf{T}_{CP,m} \mathbf{W}_{OFDM,m}^{-1} \quad (10a)$$

where  $\mathbf{W}_{OFDM,m}^{-1}$  is the  $L_{OFDM,m} \times L_{OFDM,m}$  IDFT matrix and the  $(L_{OFDM,m} + L_{CP,m}) \times L_{OFDM,m}$  CP insertion matrix is given by

$$\mathbf{T}_{CP,m} = \begin{bmatrix} \mathbf{0}_{L_{CP,m} \times (L_{OFDM,m} - L_{CP,m})} & \mathbf{I}_{L_{CP,m}} \\ & \mathbf{I}_{L_{OFDM,m}} \end{bmatrix}^T. \quad (10b)$$

Here,  $\mathbf{0}_{q \times p}$  and  $\mathbf{I}_r$  are  $q \times p$  zero matrix and  $r \times r$  identity matrix, respectively. The effective response from the  $\ell$ th OFDM subcarrier on subband  $m$  to the FC-FB output can be expressed as

$$\mathbf{f}_{\ell,m}^{(OFDM)} = \mathbf{F}_m^{(sub)} \mathbf{T}_{TX,m} \begin{bmatrix} \mathbf{0}_{1 \times \ell-1} & 1 & \mathbf{0}_{1 \times L_{OFDM,m} - \ell} \end{bmatrix}^T, \quad (11a)$$

where the  $P_m \times (L_{OFDM,m} + L_{CP,m})$  sub-matrix  $\mathbf{F}_m^{(sub)}$  with  $P_m = N_S B_{F,m}$  defining the number of useful samples in the output and  $B_{F,m} = \lceil (L_{OFDM,m} + L_{CP,m}) / L_{S,m} \rceil$  defining the number of FC processing blocks, is obtained by selecting the desired rows and columns from  $\mathbf{F}_m$  as follows:

$$[\mathbf{F}_m^{(sub)}]_{p,q} = [\mathbf{F}_m]_{p,q+S_{F,m}} \quad (11b)$$

with  $S_{F,m} = L_m - L_{S,m}$  for  $p = 1, 2, \dots, P_m$  and for  $q = 1, 2, \dots, L_{OFDM,m} + L_{CP,m}$ .

On the receiver side the OFDM processing can be expressed as

$$\mathbf{T}_{RX,m} = \mathbf{W}_{OFDM,m} \mathbf{R}_{CP,m} \quad (12a)$$

where  $\mathbf{W}_{OFDM,m}$  is the  $\bar{L}_{OFDM,m} \times \bar{L}_{OFDM,m}$  DFT matrix and the  $\bar{L}_{OFDM,m} \times (\bar{L}_{OFDM,m} + \bar{L}_{CP,m})$  CP removal matrix is given by

$$\mathbf{R}_{CP,m} = \begin{bmatrix} \mathbf{0}_{\bar{L}_{OFDM,m} \times \bar{L}_{CP,m}} & \mathbf{I}_{\bar{L}_{OFDM,m}} \end{bmatrix}. \quad (12b)$$

Now the processing response from the FC-FB input to the  $\ell$ th OFDM subcarrier can be expressed as

$$\mathbf{G}_{\ell,m}^{(OFDM)} = \mathbf{C}_m^{(\ell)} \mathbf{T}_{RX,m}^{(diag)} \mathbf{G}_m^{(sub)}, \quad (13a)$$

where the  $Q_m \times P_m$  sub-matrix  $\mathbf{G}_m^{(sub)}$  with  $Q_m = \bar{L}_{S,m} B_{G,m}$  and  $B_{G,m} = \lceil (P_m + N) / N_S - (B_{F,m})_2 \rceil$  is given by

$$[\mathbf{G}_m^{(sub)}]_{q,p} = [\mathbf{G}_m]_{q,p+S_{G,m}} \quad (13b)$$

with  $S_{G,m} = \lceil (N + [B_{G,m} - 1]N_S - P_m) / 2 \rceil$  for  $q = 1, 2, \dots, Q_m$  and for  $p = 1, 2, \dots, P_m$ . The block diagonal  $Q_m \times Q_m$  matrix  $\mathbf{T}_{RX,m}^{(diag)}$  is constructed from block diagonal  $B_{OFDM,m} \bar{L}_{OFDM,m} \times B_{OFDM,m} (\bar{L}_{OFDM,m} + \bar{L}_{CP,m})$  matrix with  $B_{OFDM,m} = \lceil Q_m / (\bar{L}_{OFDM,m} + \bar{L}_{CP,m}) \rceil$  blocks

$$\mathbf{T}_{RX,m}^{(diag)} = \text{diag}(\underbrace{\mathbf{T}_{RX,m}, \mathbf{T}_{RX,m}, \dots, \mathbf{T}_{RX,m}}_{B_{OFDM,m} \text{ blocks}}) \quad (14)$$

by selecting the first  $Q_m$  rows and columns whereas  $\mathbf{C}_m^{(\ell)}$  is the  $Q_m \times Q_m$  down-sampling by  $\bar{L}_{OFDM,m}$  with  $\ell$ -sample offset matrix.

Stemming from the above fundamental modeling, the overall processing response from the OFDM subcarrier  $\ell$  of subband  $m$  to subcarrier  $k$  of subband  $n$  can be expressed as

$$\mathbf{t}_{\ell,k}^{(m,n)} = \mathbf{G}_{k,n}^{(OFDM)} \mathbf{f}_{\ell,m}^{(OFDM)}. \quad (15)$$

Then, the passband quality on an active subcarrier  $\ell$  and on subband  $m$  can be measured using the following normalized mean-squared error (MSE) measure:

$$\text{MSE}_{\ell}^{(m)} = \left\| \mathbf{e} - \mathbf{t}_{\ell,\ell}^{(m,m)} \right\|^2 + \sum_{k=0, k \neq \ell}^{\bar{L}_{ACT,m}-1} \left\| \mathbf{t}_{\ell,k}^{(m,m)} \right\|^2 \quad (16)$$

where  $\mathbf{e} = [\mathbf{0}_{1 \times U_m} \ 1 \ \mathbf{0}_{1 \times V_m}]^T$  with  $U_m = \lceil S_{G,m} \bar{L}_m / (N \bar{L}_{OFDM,m}) \rceil$  and  $V_m = \lceil P_m / \bar{L}_{OFDM,m} \rceil - U_m$  and  $\bar{L}_{ACT,m}$  is number of active subcarriers on the receiver side on subband  $m$ . Here, the first term measures the effect of time-domain dispersion at subcarrier index  $\ell$ , resulting in general into inter-symbol interference (ISI) between  $U_m$  preceding and  $V_m$  following OFDM symbols. The second term, in turn, contains the inter-carrier interference (ICI) induced by the desired symbol,  $U_m$  preceding symbols, and  $V_m$  following OFDM symbols.

The corresponding error vector magnitude (EVM) in decibels is expressed using (16) as

$$\text{EVM}_\ell^{(m)} = 10 \log_{10} \left( \text{MSE}_\ell^{(m)} \right). \quad (17)$$

The worst-case EVM is defined as a maximum of the EVM values over the active subcarriers as given by

$$\text{EVM}_{\text{MAX}}^{(m)} = \max_{\ell=0,1,\dots,\bar{L}_{\text{ACT},m}-1} \text{EVM}_\ell^{(m)} \quad (18a)$$

whereas the average EVM is defined as the mean value of the normalized MSE values on active subcarriers, expressed in decibels as

$$\text{EVM}_{\text{AVG}}^{(m)} = 10 \log_{10} \left( \frac{1}{\bar{L}_{\text{ACT},m}} \sum_{\ell=0}^{\bar{L}_{\text{ACT},m}-1} \text{MSE}_\ell^{(m)} \right). \quad (18b)$$

Next, to quantify the in-band unwanted emissions (inside one carrier), and in particular the interference leakage between different subbands as illustrated in Fig. 4, we define the subband leakage ratio (SBLR) as the ratio of the power leaking from TX subband  $m$  to another RX subband  $n$ , within the carrier, relative to the observable RX power at subband  $m$  as

$$\text{SBLR}^{(m,n)} = 10 \log_{10} \left( \frac{P_i^{(m,n)}}{P_s^{(m)}} \right), \quad (19a)$$

where the power leaking from active subcarriers on TX subband  $m$  to the active subcarriers of the unintended RX on subband  $n$  is given as

$$P_i^{(m,n)} = \sum_{\ell=0}^{L_{\text{ACT},n}-1} \sum_{\bar{k}=0}^{\bar{L}_{\text{ACT},m}-1} \left\| \mathbf{t}_{\ell,\bar{k}}^{(m,n)} \right\|^2 \quad (19b)$$

and the observable reference power on the active subcarriers on target RX subband  $m$  is defined as

$$P_s^{(m)} = \sum_{\ell=0}^{L_{\text{ACT},m}-1} \sum_{\bar{k}=0}^{\bar{L}_{\text{ACT},m}-1} \left\| \mathbf{t}_{\ell,\bar{k}}^{(m,m)} \right\|^2. \quad (19c)$$

In the actual FC-based subband filter optimization, we use the minimum stopband attenuation of the synthesis processing as a figure of merit for the subband band-limitation characteristics, since this measure gives an straightforward way to control the power leaking to adjacent subband independent of RX processing and the number of used guard subcarriers. The magnitude squared response of the synthesis processing is given by

$$M(\omega) = \frac{1}{N\lambda} \sum_{n=0}^{N\lambda-1} |F_m^{(n)}(e^{j\omega})|^2, \quad (20)$$

where the frequency responses  $F_m^{(n)}(e^{j\omega})$  are evaluated using the impulse responses given by the  $N\lambda$  time-variant columns of the matrix  $\mathbf{F}_m$  as given by (4).

The FC-filtered F-OFDM system design can now be stated as an optimization problem for finding the optimal values of the frequency-domain window ( $L_{\text{TBW},m}$  non-trivial values of  $\mathbf{D}_m$  in (9)) to

$$\begin{aligned} & \underset{d_{0,m}, d_{1,m}, \dots, d_{L_{\text{TBW},m}-1,m}}{\text{minimize}} && \text{EVM}_{\text{MAX}}^{(m)} \\ & \text{subject to} && M(\omega) \leq A_s, \quad \text{for } \omega \in \Omega_s, \end{aligned}$$

where  $A_s$  is the desired minimum stopband attenuation and  $\Omega_s$  is the stopband region. This problem can be straightforwardly solved using non-linear optimization algorithms since the number of optimized parameters is typically low (no more than seven in the examples considered in this paper) when taking into account that only the transition band weights are used in the optimization. Notice that by varying the value of  $A_s$  in the optimization, the SBLR and OOB emissions can be directly controlled.

Due to the complexity of the system model, it is practically impossible to prove the convexity of the optimization problem through analytical means, and therefore, strictly speaking, the global optimality of the solution cannot be guaranteed. However, our studies using several different starting points for the optimization and using different numerical algorithms have shown that the optimization converges reliably to same solution and, therefore, we can assume optimum is also the global one.

It should be noted that we are not targeting to reach perfectly linear convolution through FC processing, but our goal in the design is to keep the cyclic distortion effects at a level that does not significantly impact the link error rate performance, such that the non-implementation-related effects are dominating. The main cause for EVM degradation is the partial suppression of sidelobes of subcarriers close to the subband edges, which is unavoidable in F-OFDM. In contrast to earlier schemes, this effect is directly minimized by our design approach.

### C. 5G-NR Numerology and FC-FB Parametrization

Considering the FC-F-OFDM transmitter in Fig. 5, it was assumed in [8] that the short FFT-length in FC processing is the same as the IFFT length in OFDM processing. In [9], this constraint is relaxed and it is assumed that the two transform lengths can be chosen independently. Considering the mixed numerology cases, we choose  $N = \max\{N_{\text{OFDM},m}\}$ , where  $N_{\text{OFDM},m}$  is the OFDM symbol duration in subband  $m$  in high-rate samples,  $f_s/N_{\text{OFDM},m}$  is the corresponding SCS, and  $f_s$  is the high sampling rate. In the structure of Fig. 5, the OFDM processing module generates useful symbol duration of  $L_{\text{OFDM},m}$  and the inserted CP-length is denoted as  $L_{\text{CP},m}$ . The FC-filtering process increases the sampling rate by the factor of  $N/L_m$ , resulting in overall symbol duration of  $N_{\text{OVR}} = N(L_{\text{OFDM},m} + L_{\text{CP},m})/L_m = N_{\text{OFDM},m} + N_{\text{CP},m}$ . Here  $L_{\text{OFDM},m}$  and  $L_{\text{CP},m}$  need to take integer values. It is convenient, but not necessary, that  $N_{\text{OFDM}}$  and  $N_{\text{CP}}$  take integer values as well. In the flexible numerology considered for 3GPP 5G-NR, the SCS is an integer power of two times 15 kHz, say  $2^\eta \times 15$  kHz. Then one natural choice is  $N = N_{\text{OFDM}}$  in the basic case with 15 kHz SCS and  $N_{\text{OFDM}} = N/2^\eta$  generally.

As a concrete example, we focus here on a 10 MHz 5G-NR like multicarrier system utilizing CP-OFDM baseline waveform. The long transform length on the transmitter and receiver sides is fixed to  $N = 1024$ . The sampling rate is  $f_s = 15.36$  MHz with  $N_{\text{OFDM}} = N/2^\eta = 1024/2^\eta$  and  $N_{\text{CP}} = 72/2^\eta$ . Table I shows example numerologies for SCSs of 15 kHz and 30 kHz. The active subcarriers are always scheduled in PRBs of 12 subcarriers. We notice that with

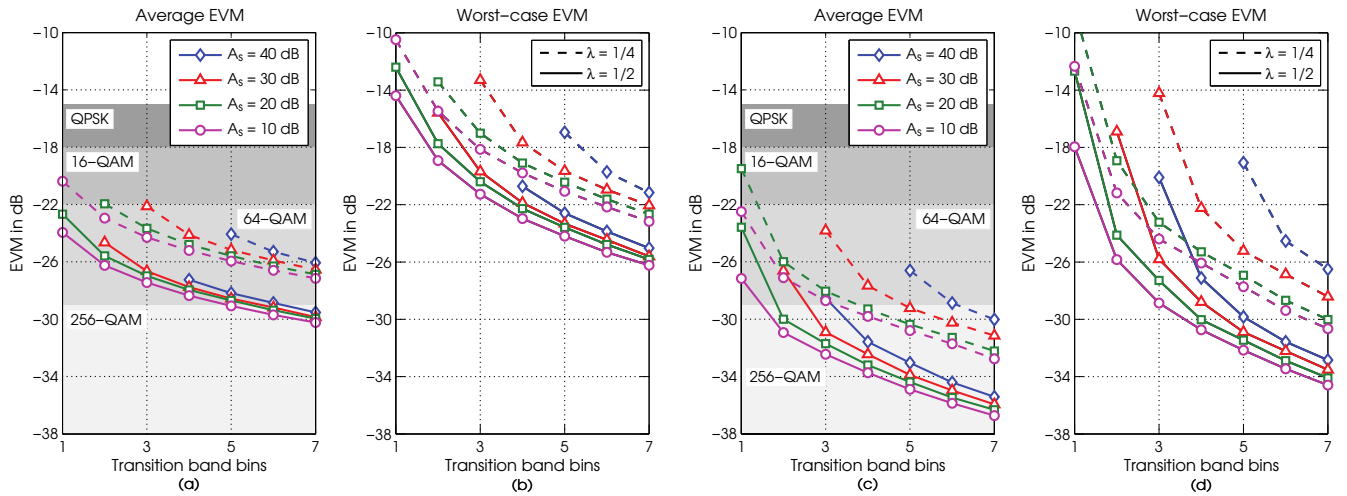


Fig. 6: Average and worst-case EVMs as a function of transition bandwidth for a filtered group of 4 PRBs with different minimum stopband attenuation levels and 25% and 50% FC overlaps. (a)-(b): Wideband TX, RX filtering only. (c)-(d): Isolated group of 4 PRBs with both TX and RX filtering.

TABLE I: Example parametrizations for FC-F-OFDM based 5G physical layer with 10 MHz carrier bandwidth

| SCS    | No. act. subcar. | $N$  | $L_{\text{OFDM},m}$ | $L_{\text{CP},m}$ | $L_m$ |
|--------|------------------|------|---------------------|-------------------|-------|
| 15 kHz | 12 (1 PRB)       | 1024 | 128                 | 9                 | 128   |
| 15 kHz | 48 (4 PRBs)      | 1024 | 128                 | 9                 | 128   |
| 15 kHz | 600 (50 PRBs)    | 1024 | 1024                | 72                | 1024  |
| 30 kHz | 12 (1 PRB)       | 1024 | 128                 | 9                 | 256   |
| 30 kHz | 24 (2 PRBs)      | 1024 | 128                 | 9                 | 256   |
| 30 kHz | 300 (25 PRBs)    | 1024 | 512                 | 36                | 1024  |

narrow allocations, the short transform lengths are limited by the integer CP length constraint. While mixed numerology cases with wider SCS will be considered in Section V, in the numerical examples of this section we focus on the basic case with  $\eta = 0$ .

It should be noted that in 5G numerology proposals, the length of the first CP is different from the other ones. The symbol boundary alignment is done within 0.5 ms intervals. With 15 kHz SCS, the first CP is extended in the 50 PRB case by 8 samples to 80 and in the 1 PRB and 4 PRB cases to 10 samples. Then a 0.5 ms subframe corresponds exactly to 15 FC processing blocks with 50% overlap and to 10 FC processing blocks with 25% overlap. The same applies for higher SCSs while the overall number of OFDM symbols in a subframe is proportional to  $2^\eta$ .

#### D. Numerical Results for Passband EVM and Adjacent Subband SBLR

Here we evaluate first the passband EVM and adjacent subband SBLR characteristics of FC-F-OFDM subband filtering for the 4-PRB configuration of Table I with different filter transition bandwidths and two FC overlap factors,  $\lambda = 1/2$  or  $\lambda = 1/4$ . In these evaluations, the worst-case and average EVMs, as given by (18a) and (18b), are used as measures of the passband quality while the SBLR directly quantifies how much interference leakage there is between the neighboring subbands. The results are shown in Figs. 6 (a)–(b) for the case where a full-band CP-OFDM signal is transmitted and optimized subband filtering is done only on the RX side. The

targeted group of 4 PRBs is in the central part of the carrier, such that adjacent PRB groups are present in the received signal. This can be seen as a basic unmatched filtering case, which is relevant for narrowband low-power machine type communications (MTC) receivers. The corresponding results can be seen in Figs. 6(c)–(d) for the case where matched subband filtering is done on both TX and RX sides for an isolated group of 4 PRBs. Figs. 6(a),(c) show the average passband EVMs and Figs. 6(b),(d) show the worst-case EVMs as a function of the filter transition bandwidth expressed in FFT bin spacings and for cases where the lowest stopband attenuation levels (typically at the stopband edges) are at  $A_s = \{10, 20, 30, 40\}$  dB.

We can see that the FC overlap factor has quite significant effect on the performance. For narrow transition bandwidths, the tradeoff between EVM and minimum stopband attenuation is clear, whereas for wider transition bands, reduced stopband attenuation does not help to improve the passband performance significantly. The worst-case EVM is considerably higher than the average. This is obviously due to the fact that on the edge subcarriers, the strict orthogonality is impaired. This contribution to average EVM is more severe with narrowband allocations.

These results can be evaluated in the context of the EVM requirements of LTE, stated as  $\{17.5\%, 12.5\%, 8\%, 3.5\%\}$  or  $\{-15\text{ dB}, -18\text{ dB}, -22\text{ dB}, -29\text{ dB}\}$  for  $\{\text{QPSK}, 16\text{-QAM}, 64\text{-QAM}, 256\text{-QAM}\}$  modulations, respectively. We also respect the idea that the filtering effects should consume only a relatively small part of the stated EVM targets, to leave room for EVM degradation due to RF components. Then we can see that, with  $\lambda = 1/2$ , even transition band of 1 FFT bin can be considered sufficient for QPSK from the average EVM point of view. For 64-QAM, transition band of 2 FFT bins is enough, also with one-sided filtering in the average EVM sense. For 256-QAM, 2 FFT bin transition band is sufficient in the two-sided filtering case to achieve average EVM below  $-29$  dB, while 7 FFT bin transition band is required in the RX filtering only case.



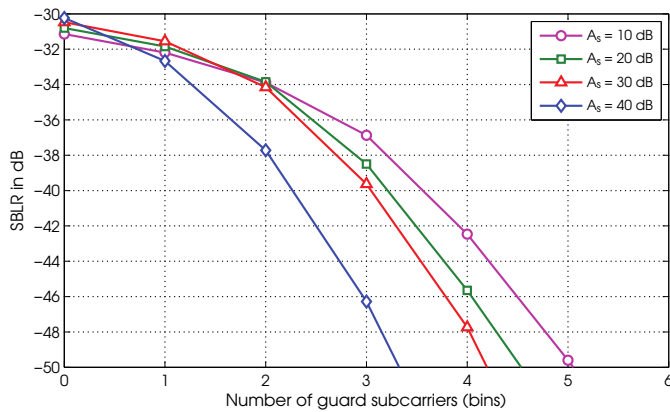


Fig. 7: SBLR as a function of the number of guard subcarriers between two adjacent subbands of 4 PRBs.

Similar study on the 1 PRB allocation shows that the average EVM values are about 5 dB higher than in 4 PRB subband case and the worst-case values are 1–2 dB higher. Typically, 1 PRB transmissions are used only on cell edge in coverage limited scenarios, in which the used modulation is most likely QPSK and not limited by the FC processing induced passband EVM. In the full-band case, with 50 PRB filtering band, the average EVM is in the order of  $-40$  dB, more than 10 dB lower than in the 4 PRB case, and also the worst-case EVMs are improved by 3–4 dB.

Fig. 7 shows the corresponding SBLR, evaluated using (19), as function of the guard subcarriers between two adjacent 4-PRB subbands. As can be observed from this figure, the SBLR is well below  $-30$  dB without any guard subcarriers between the subbands and reaches  $-45$  dB with only 3–5 subcarrier guardband. In addition, it can be seen that the required minimum stopband attenuation in the optimization controls perfectly the subband band-limitation characteristics as desired. Now given the target EVM for the desired modulation and coding scheme (MCS) to be supported, one can select the parameter set that fulfills the passband EVM target and then evaluate the SBLR with different number of guard subcarriers to find out the required guard band to support the desired MCS.

Two examples of power spectral density (PSD) plots for FC filtered OFDM with 50 active PRBs are shown in Figs. 8(a) and 8(c). In Fig. 8(a) the overlap factor in FC processing is  $\lambda = 1/2$  and the minimum stopband attenuation is  $A_s = 20$  dB whereas in Fig. 8(c) the overlap factor is  $\lambda = 1/4$  and the minimum stopband attenuation is  $A_s = 40$  dB. Figs. 8(b) and 8(d) show the simulated EVMs on active subcarriers as well as the squared magnitude responses of the AFBs. In Figs. 8(b) and 8(d) the number of active PRBs on the receiver side are 4 and 50, respectively.

#### IV. LINK-LEVEL PERFORMANCE EVALUATIONS AT SUB-6 GHz FREQUENCY BANDS

In this section, performance results for FC filtered CP-OFDM and DFT-spread-OFDM (DFT-s-OFDM) radio links are presented in terms of PSD, EVM, and block error rate (BLER) performance. In addition, the FC-F-OFDM waveform

is compared against several different 5G candidate waveforms, including traditional CP-OFDM without any windowing or filtering which is used as a reference, WOLA [30], universally filtered OFDM with CP (CP-UF-OFDM) [3], [10], and f-OFDM [6].

##### A. Reference Waveforms

With CP-UF-OFDM [3], [10], the used filter is a Dolph-Chebyshev finite impulse response (FIR) filter of length  $N_{\text{FIR}}$  and the stopband attenuation is a design parameter defining also the the 3 dB-passband width of the filter. The UF-OFDM processing was initially developed for zero-prefix OFDM, but it can be equally well used with CP-OFDM [10]. The CP-UF-OFDM design ideology relies on a small number of different, predesigned filters typically optimized for 1, 2, or 4 PRB subbands. In the later performance examples with 15 kHz SCS and 4-PRB subbands, filter stopband attenuations of 75 dB and 37 dB are used with  $N_{\text{FIR}} = 73$  and  $N_{\text{FIR}} = 37$ , respectively. With 30 kHz SCS and 2-PRB subbands, the stopband attenuations of 37 dB and 30 dB are used with  $N_{\text{FIR}} = 73$  and  $N_{\text{FIR}} = 37$ , respectively. TX side pre-equalization is used to remove the TX filter effect on the amplitude response, and on the RX side, corresponding equalization is used to compensate the RX filter passband attenuation.

The f-OFDM was introduced in [6]. The used filter is based on Hann-windowed sinc-function, where the sinc-function is defined based on the allocation bandwidth. The filter length is  $N_{\text{FIR}} = 512$ . The filter is separately designed for different subband widths by tuning the sinc-function spectral width to match the allocation width. Because the main sinc-pulse length in time depends on the allocation width, the assumed filter causes minimal ISI with wide allocations but may cause significant ISI with narrow allocations, e.g., 1 PRB allocation. The subband wise filtering is performed in both, TX and RX, and the RX filter is matched to the TX filter. TX side subband-wise pre-equalization and RX-side compensation is used to alleviate the EVM increase caused by passband attenuation with f-OFDM. Typically, a tone offset (TO) is defined for f-OFDM. TO defines the passband width extension as an integer multiple of the used SCS. In the presented results it is assumed that TO is either 0 or 4 depending on the simulation case, as explained later.

The WOLA processing with CP-OFDM or DFT-s-OFDM is a widely known, computationally efficient method to improve the spectral containment of a CP-OFDM signal [31], [30]. It has been introduced for 5G-NR as a low-complexity candidate method to allow improved SBLR to support mixed numerology and asynchronous traffic. In the presented results, only the simple single window scheme is assumed. Enhanced versions of WOLA exist, and their potential impacts will be briefly discussed at the end of Section IV-I.

In WOLA, the CP-OFDM symbol is extended by  $N_{\text{EXT}}$  samples, and the number of extended samples equals to the window slope length  $N_{\text{WS}} = N_{\text{EXT}}$ . Window slope length defines in samples the rising and falling edge of the window. The window slope length used in the simulations is  $N_{\text{WS}} = N_{\text{CP}} = 72$ . This value is chosen to provide as good spectral

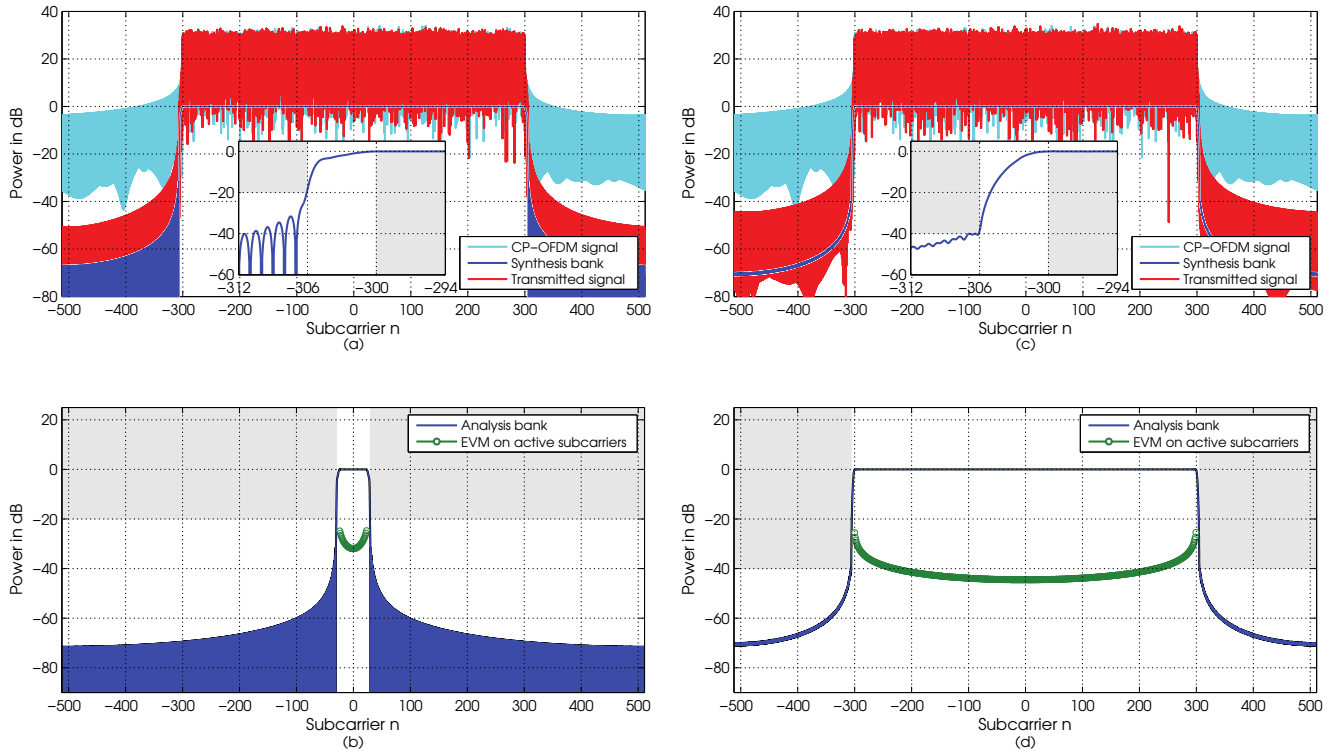


Fig. 8: Upper figures: PSD of the generated FC-filtered OFDM signal in the case of 50 active PRBs. Lower figures: Simulated active subcarrier EVM for two different RX configurations. Also the analysis and synthesis filter bank responses are shown in these figures. In these cases, six transition band FFT bins are used. (a)-(b) The overlap in FC processing is 50% and the required minimum stopband attenuation is  $A_s = 20$  dB. The number of active PRBs on the RX side is 4. (c)-(d) The overlap in FC processing is 25% and the required minimum stopband attenuation is  $A_s = 40$  dB. The number of active PRBs on the RX side is 50.

containment as possible without significant degradation in the passband EVM after the power amplifier (PA). The total window length in TX is  $N_{\text{WIN,TX}} = N_{\text{FFT}} + N_{\text{CP}} + N_{\text{WS}}$ . After windowing, an overlap-and-add processing is used to partially overlap adjacent windowed CP-OFDM symbols by  $N_{\text{EXT}}$  samples to reduce the overhead caused by windowing and to retain the original symbol timing. The used window is a raised cosine (RC) window with roll-off of  $N_{\text{WS}}/N_{\text{WIN}}$  [32]. In the RX side, the WOLA processing is performed within the CP-OFDM symbol boundaries. The used window length is  $N_{\text{WIN,RX}} = N_{\text{FFT}} + N_{\text{WS}}$ . In other words, in RX side the received CP-OFDM symbol is not extended before WOLA processing, as indicated also in [30].

### B. Simulation Cases, Assumptions, and Performance Metrics

In 3GPP TSG-RAN WG1 way forward agreement it has been agreed that CP-OFDM is the baseline waveform for 5G-NR physical layer [13]. Therefore, all downlink (DL) and UL performance results are based on subband-filtered CP-OFDM signals. In [33], also DFT-spread-OFDM was agreed to be supported in UL in coverage limited scenarios. In Section IV-H, examples of FC filtered DFT-spread-OFDM signal are also given.

The baseline physical layer definition and numerology follows the one defined for LTE operating in a 10 MHz channel. The main evaluation parameters are given in Table II. As observed in Fig. 6, optimized FC design with TBW of 2 FFT

bins and minimum stopband attenuation level  $A_s = 10$  dB is sufficient to achieve average MSEs below  $-29$  dB, required for 256-QAM [34]. The values of Table II are used unless stated otherwise.

All the presented results assume an ideal channel knowledge in the RX and each simulated subframe contains only data symbols. A guard period is added to each subframe to allow rising and falling transients caused by filtering or windowing to take place. If filtering causes transients longer than the guard period, they are truncated with a RC window to fit within the subframe. The link performance is evaluated in TDL-C channels [35] with 300 ns and 1000 ns root mean squared (RMS) delay spread. In TDL channels the RMS delay spread is defined by a scaling factor indicated in the name.

The link performance results are provided for DL and UL following the simulation cases defined in [14, Annex A]. *Case 1a* corresponds to interference free DL scenario and *Case 1b* corresponds to interference free UL scenarios, *Case 2* defines a mixed numerology DL scenario, *Case 3* defines an asynchronous UL scenario, and *Case 4* defines a mixed numerology UL scenario. In all the simulations, the target signal has a SCS of 15 kHz. In *Case 2* and *Case 4*, the interfering signal has SCS of 30 kHz. In *Case 3*, the interfering signal has the same SCS as the target signal, but it is time shifted with 128 samples to model asynchronous interference. In all cases with interfering signal present, the interfering signal is assumed to be processed in similar manner

TABLE II: Main evaluation parameters.

| Parameter                             | Value                         |
|---------------------------------------|-------------------------------|
| Carrier frequency                     | 4 GHz                         |
| UE mobility                           | 3 km/h                        |
| Channel bandwidth                     | 10 MHz                        |
| Sampling frequency                    | 15.36 MHz                     |
| Channel model                         | TDL-C [35]                    |
| DL PA model                           | Modified Rapp [36]            |
| IBO in DL                             | 11.6 dB                       |
| UL PA model                           | Polynomial model [37]         |
| Desired signal IBO in UL              | 8 dB                          |
| Interfering signal IBO in UL          | 5.5 dB                        |
| Channel codec                         | Turbo code [38]               |
| Guard period length at high rate      | 72 samples                    |
| Subband allocation granularity        | 720 kHz                       |
| FC block length                       | $N = 1024$ samples            |
| Overlap factor in FC processing       | 1/2                           |
| Transition bandwidth in FC processing | $L_{TBW} = 2$                 |
| Minimum stopband attenuation target   | $A_s = 10$ dB                 |
| Target OFDM symbol length             | $N_{OFDM} = 1024$ samples     |
| Target signal CP length               | 72 samples                    |
| Target signal subcarrier spacing      | 15 kHz                        |
| Interfering OFDM symbol length        | $N_{OFDM} = 1024/512$ samples |
| Interfering signal CP length          | 72/36 samples                 |
| Interfering signal subcarrier spacing | 15/30 kHz                     |
| OFDM symbols per subframe             | 14/28                         |

as the evaluated waveform. In the mixed numerology scenarios (*Case 2* and *Case 4*) and asynchronous interference scenario (*Case 3*), guard band (GB) defines the increase in the distance of the edge-most SC centers with respect to the minimum 15 kHz distance.

The presented EVM results are evaluated by inserting the PA input or output signal to a waveform specific detector. No equalization is applied in the presented EVM results. In the evaluation of the EVM, with f-OFDM and CP-UF-OFDM, the FFT window is located at the center of the CP-OFDM symbol in TDL-C 300 ns channel and in the end of the CP-OFDM symbol in TDL-C 1000 ns channel. This shifting of the RX FFT window reduces the filtering induced ISI in the TDL-C 300 ns channel to provide a realistic performance comparison between waveform candidates. In practice, to support this the RX has to have capability to estimate channel delay profile and adjust the RX FFT window location per subband. With WOLA, due to long window and the RX WOLA processing, the FFT window is always located in the middle of the CP-OFDM symbol after RX WOLA processing. With FC-F-OFDM, the RX FFT window is always in the end of the CP-OFDM symbol.

The PSD is evaluated per subframe. In the presented results, 100 independent realizations at the PA output are averaged and filtered to model 30 kHz measurement bandwidth used to define the LTE out-of-band emission mask (OOBEM) within 1 MHz distance from the channel edge in DL and UL. The DL OOBEM is defined in [34] and UL OOBEM is defined in [39]. These are commonly agreed as a starting point for evaluating the OOB emissions for new waveform candidates in 5G-NR.

### C. Power Amplifier Models

The PA models used in this paper have been introduced for performance evaluations for below 6 GHz communications in 3GPP TSG-RAN WG1. The DL PA model was introduced in

[36] and UL PA model in [37]. These models are used because they are openly available and commonly agreed to provide a good starting point for spectral containment evaluations related to 5G-NR.

The DL PA model is a modified Rapp model [36]. It mimics a base station (BS) PA including some crest factor reduction and digital predistortion schemes to linearize the BS PA to achieve the LTE OOBEM and OOB adjacent channel leakage ratio (ACLR) of 45 dB with a fully populated 10 MHz LTE signal with 50 PRBs and 64-QAM modulation. The modified Rapp model is defined by the amplitude-to-amplitude (AM-AM) distortion

$$F_{AM-AM}(x) = \frac{G}{\left(1 + \left|\frac{Gx}{V_{SAT}}\right|^{2p}\right)^{1/(2p)}}, \quad (21a)$$

and amplitude-to-phase (AM-PM) distortion

$$F_{AM-PM}(x) = \frac{A \left|\frac{Gx}{V_{SAT}}\right|^q}{1 + \left|\frac{Gx}{BV_{SAT}}\right|^q}, \quad (21b)$$

where  $x$  is the instantaneous amplitude of the signal, gain is normalized to  $G = 1$ , saturation voltage is  $V_{SAT} = 239.6$  at 50  $\Omega$  load, smoothness factors are  $p = 3$  and  $q = 5$ , and tuning parameters are  $A = -0.14$  and  $B = 1.2$ . This model has a 1 dB compression point at  $P_{1dB} = 57.6$  dBm. A backoff of 11.6 dB is assumed for simulations, providing  $P_{DL} = 46$  dBm total output power from the PA.

The UL PA model is a polynomial model of order nine obtained by fitting the polynomial to measurements from a commercial PA [37]. The polynomial coefficients are ordered from  $p_9$  to  $p_0$ , given in logarithmic domain, and defined for the amplitude distortion as

$$p_{AM} = [7.9726 \times 10^{-12}, 1.2771 \times 10^{-9}, 8.2526 \times 10^{-8}, 2.6615 \times 10^{-6}, 3.9727 \times 10^{-5}, 2.7715 \times 10^{-5}, -7.1100 \times 10^{-3}, -7.9183 \times 10^{-2}, 8.2921 \times 10^{-1}, 27.3535], \quad (22a)$$

and for phase distortion as

$$p_{PM} = [9.8591 \times 10^{-11}, 1.3544 \times 10^{-8}, 7.2970 \times 10^{-7}, 1.8757 \times 10^{-5}, 1.9730 \times 10^{-4}, -7.5352 \times 10^{-4}, -3.6477 \times 10^{-2}, -2.7752 \times 10^{-1}, -1.6672 \times 10^{-2}, 79.1553]. \quad (22b)$$

The polynomial model should be used only with input levels between -30 dBm and 9 dBm. The input referred 1 dB compression point is at  $P_{1dB} = 3.4$  dBm and the model is parametrized to provide 26 dBm PA output power with 20 MHz quadrature phase-shift keying (QPSK) modulated fully populated LTE uplink signal (100 PRB allocation), while meeting the minimum ACLR requirement of 30 dB for evolved UMTS terrestrial radio access (E-UTRA) and UL emission masks.

Below, all PSD and link performance results are obtained with the stated PA models, while EVM results are given for both PA input and output signals to illustrate the PA induced error. All EVM and link performance results are for matched

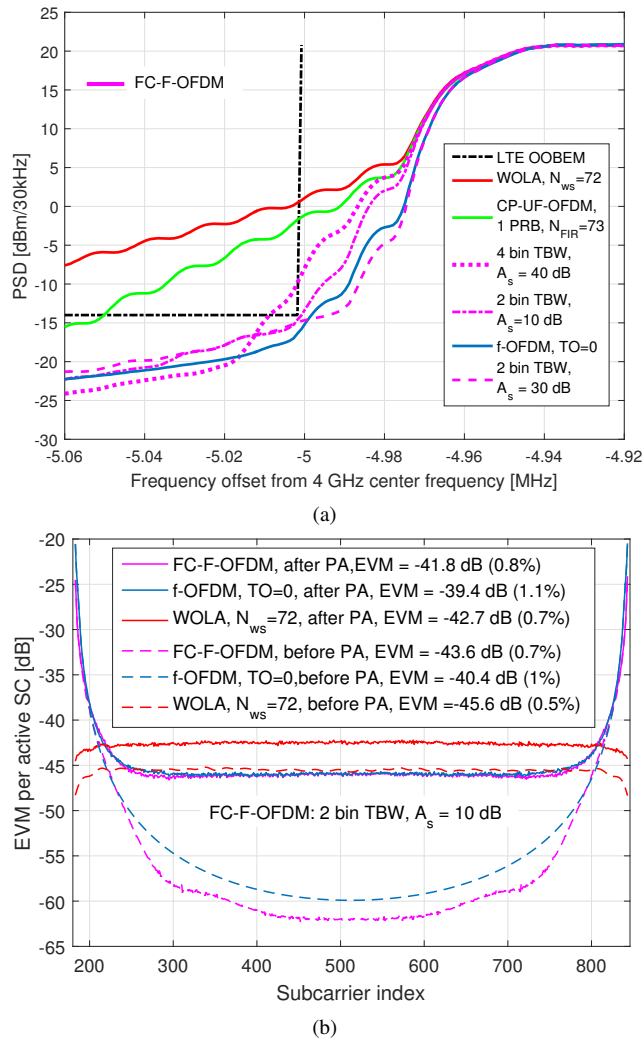


Fig. 9: Results for 55 PRB allocation in a 10MHz channel with different enhanced CP-OFDM waveforms. (a) Channel edge PSD with DL PA model. (b) Subcarrier wise EVM results with and without the DL PA model.

TX and RX filtering cases. The numerical EVM values given below are for average EVM over the active subcarriers, unless otherwise noted.

#### D. Case 1: Interference free DL and UL link performance

In 3GPP TSG-RAN WG1 physical layer way forward agreement [13] it has been decided that 5G-NR should support higher bandwidth efficiency than the current LTE technology. Therefore, we start by evaluating the FC-F-OFDM performance in the given 10 MHz channel with 55 PRB allocation. The current LTE technology supports 50 PRBs in a 10 MHz channel. Increasing the maximum number of supported PRBs per channel increases the filtering requirements and emphasizes the channel filter design required to achieve the current LTE-based OOBEM requirements. At the same time, the EVM degradation of the edge PRBs should be included in the evaluation because it would limit the MCS range that can be applied in these PRBs.

In Fig. 9, the performance of the FC-F-OFDM is compared against f-OFDM and WOLA in terms of (a) PSD and (b) passband EVM. The results are shown assuming a 55 PRB

allocation in a 10MHz LTE channel. In this example, the bandwidth utilization efficiency is 99% and there is only 100 kHz GB between channel edge and first PRB. As expected, FC-F-OFDM with 4 bin TBW already violates the OOBEM. Also, for 3 bin TBW no optimized weights were found achieving the OOBEM. With 2 bin TBW, both attenuation targets  $A_s = 10$  dB and  $A_s = 30$  dB achieve the defined OOBEM. The 2 bin TBW with  $A_s = 10$  dB design is the best choice when noting the clear improvement in the passband EVM. These results also give an example how the attenuation target in the optimization can be used to fine-tune the tradeoff between frequency selectivity and passband EVM. With 2 bin TBW and  $A_s = 30$  dB, the filtered signal is well within the emission mask but the EVM is  $-37.1$  dB (1.4%). By reducing design attenuation target to  $A_s = 10$  dB, the 2 bin TBW EVM can be reduced to  $-41.8$  dB (0.8%), while fulfilling the OOBEM.

When the bandwidth efficiency is increased from 50 PRBs, WOLA is unable to suppress the OOB emissions sufficiently and needs to be combined with some additional channel filtering to fulfill the OOBEM. This indicates that simple WOLA processing alone is not sufficient to support increased bandwidth utilization efficiency expected from 5G-NR. Similar observations can be made for CP-UF-OFDM, for which the example PSD is obtained with 1 PRB subband filter with 20 dB stopband attenuation. The f-OFDM performance is between the 2 bin TBW cases presented in Fig. 9 (a). WOLA provides the best average passband EVM performance, FC-F-OFDM achieves almost the same, and f-OFDM has the largest EVM while being still sufficiently low to support fullband transmission with 256-QAM modulation. At the edges of the channel a clear degradation on the EVM is observed for FC-F-OFDM and f-OFDM due to the steep filtering. WOLA has significantly better EVM at channel edges and it is in fact decreasing towards the channel edges. In the first PRB, the average EVM for FC-F-OFDM is  $-30.2$  dB and for f-OFDM it is  $-26.6$  dB. This indicates that FC-F-OFDM allows to use 256-QAM modulation in all PRBs, whereas with f-OFDM the edge-most PRBs are limited to 64-QAM modulation.

In the TDL-C 300 ns channel, all waveform candidates perform well in DL with MCS 256-QAM,  $R = 4/5$  with allocations sizes from 4 PRBs up to 55 PRBs. In UL all waveform candidates work up to MCS 64-QAM,  $R = 3/4$ . Higher MCSs do not work in UL due to the passband distortion generated by the polynomial PA model with the used 8 dB input backoff. In the TDL-C 1000 ns channel differences between waveform candidates become more clear as the channel induced ISI starts to have a significant role. In Fig. 10 the link performance for different waveform candidates in (a) DL and (b) UL are shown for MCS 64-QAM,  $R = 3/4$ . In the presented results, f-OFDM with TO of 4 provides performance closest to the reference CP-OFDM. FC-F-OFDM and CP-UF-OFDM with  $N_{FIR} = 37$  provide similar performance and are very close to the reference CP-OFDM at BLER target of 10% but diverge further at BLER target of 1%. WOLA and f-OFDM with TO of 0 lose approximately 2 dB to other waveform candidates at BLER target of 10% and do not achieve BLER target of 1%. With WOLA, the TX and RX processing with long window



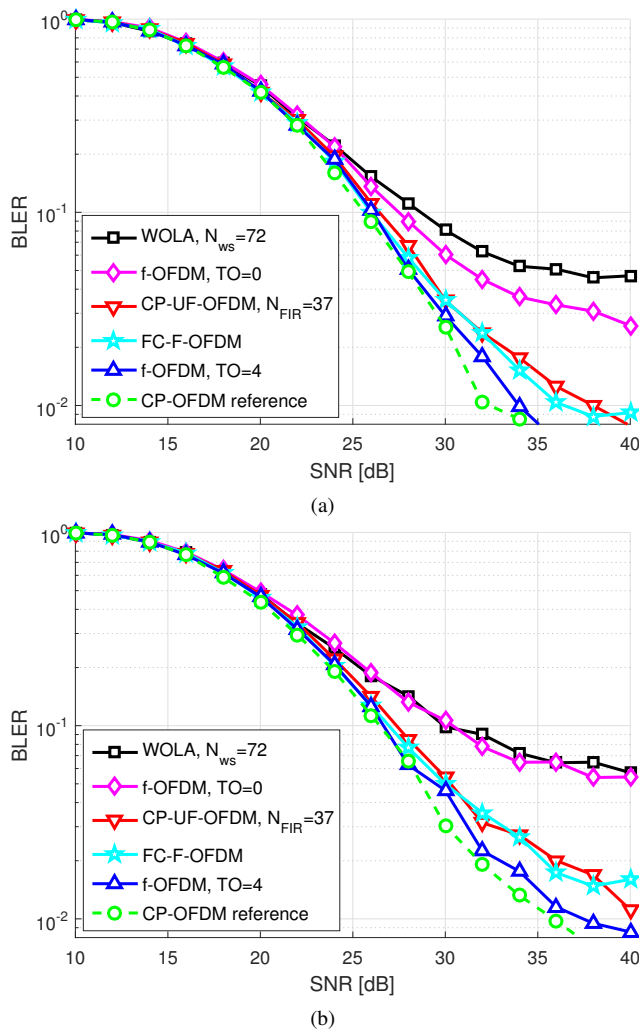


Fig. 10: Performance comparison for (a) *Case 1a* (DL) and (b) *Case 1b* (UL) with 4 PRB allocation.

slope length spreads the channel induced ISI which leads to degraded performance. This effect could be reduced with shorter RX window lengths. With f-OFDM, increasing the TO reduces the passband distortion caused by the subband filtering in this scenario. On the other hand, the mentioned methods for enhancing the passband performance of WOLA and f-OFDM reduce the spectral containment and degrade the performance in the following simulation cases where an interfering signal is introduced to the vicinity of the target signal.

#### E. Case 2: Mixed numerology DL link performance

In Fig. 11, the *Case 2* DL scenario is evaluated in the TDL-C 300 ns channel with MCS 256-QAM,  $R = 3/4$ . The effect of GB with two different FC TBWs and  $A_s = 10$  dB are shown in Fig. 11 (a) and the link performance of all candidate waveforms assuming a GB=30 kHz are shown in Fig. 11 (b). In this DL scenario, the required GB is typically smaller than in the corresponding UL scenario and it supports higher MCS due to the more linear PA model. It can be seen that a GB of 30 kHz is sufficient to achieve interference free performance with FC-F-OFDM. Furthermore, with the same GB, FC-F-OFDM provides the best link performance among all waveform candidates.

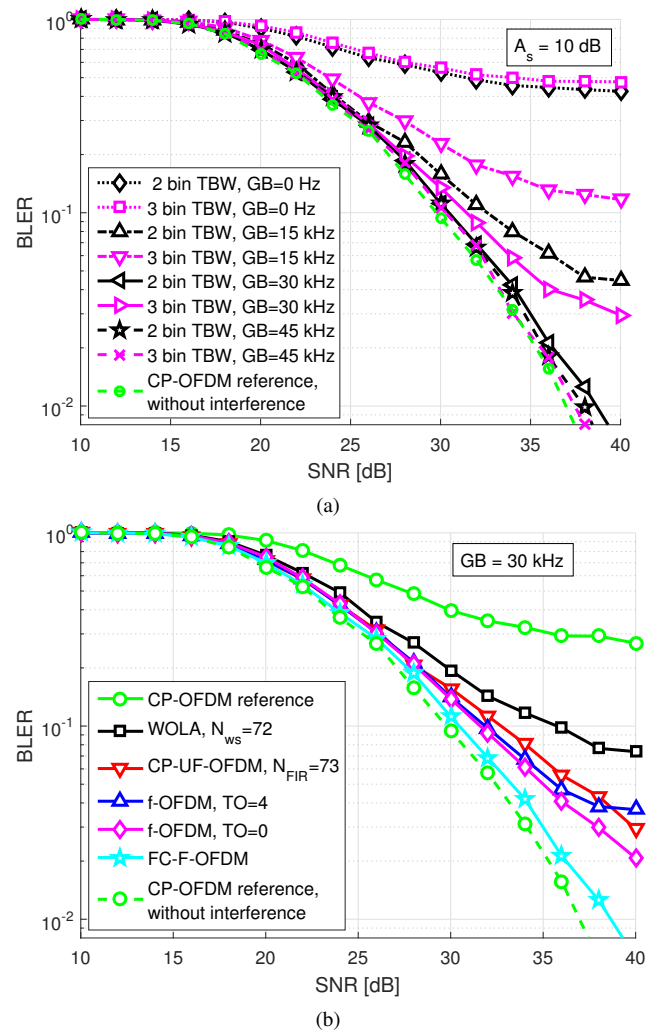


Fig. 11: Performance comparison for *Case 2* mixed numerology DL scenario in TDL-C 300 ns channel. (a) FC-F-OFDM performance with different GB values. (b) The relative performance with different waveforms with GB = 30 kHz.

In Fig. 12, the *Case 2* scenario is evaluated in the TDL-C 1000 ns channel with MCS 64-QAM,  $R = 3/4$ . The outcomes of the evaluation are similar as for TDL-C 300 ns channel: GB of 30 kHz is sufficient to isolate the interference between different numerologies with FC-F-OFDM and that FC-F-OFDM provides the best link performance with this GB. In TDL-C 1000 ns channel the difference between FC-F-OFDM and other waveform candidates grows even bigger, showing a 2 dB difference to closest candidate at BLER target of 10%.

#### F. Case 3: Asynchronous UL link performance

In *Case 3* and *Case 4* simulations, the target signal uses MCS 64-QAM,  $R = 1/2$ , with input back-off (IBO) of 8 dB which leads to 22.5 dBm PA output power, and the interfering signals use MCS QPSK,  $R = 1/2$  with IBO of 5.5 dB which leads to 24.7 dBm PA output power. These IBO values were chosen in such a manner that the in-band emission mask and OOBEMs are fulfilled for the desired and interfering signals, assuming a 50 PRB maximum allocation in the channel and evaluating separately either desired or interfering signal at the channel edge. The interfering signal was chosen to have lower

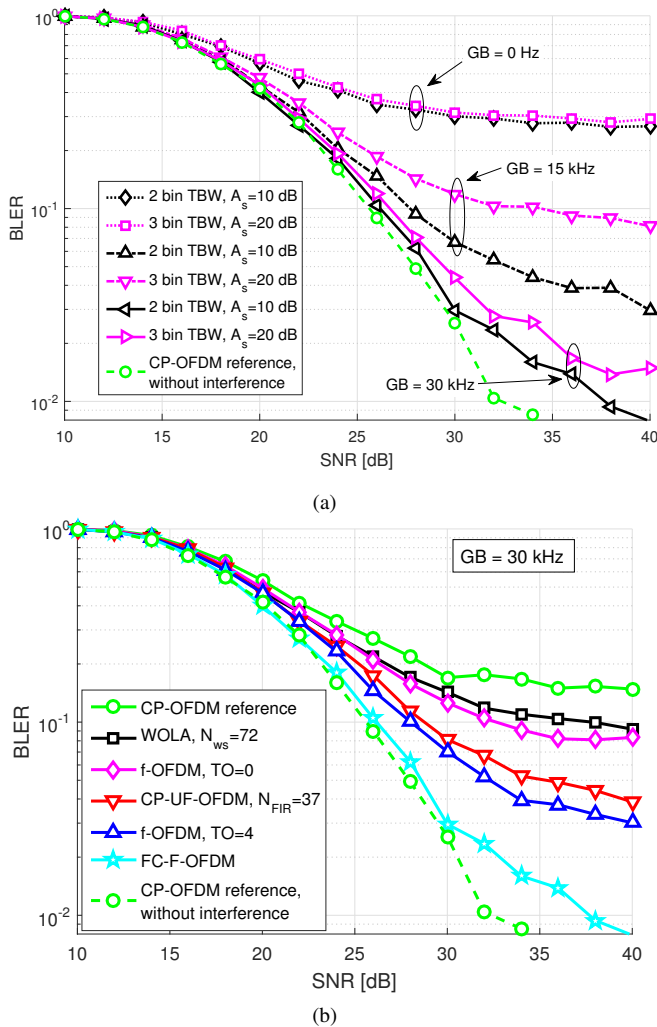


Fig. 12: Performance comparison for *Case 2* mixed numerology DL scenario in TD-LC 1000 ns channel. (a) FC-F-OFDM performance with different GB values and parameterizations. (b) Relative performance with different waveforms with GB = 30 kHz.

MCS and lower IBO because this maximizes the interference leakage from the interfering signal and can be considered as the worst case scenario.

In Fig. 13, the link performance in *Case 3* asynchronous UL in TD-LC 1000 ns channel with MCS 64-QAM,  $R = 1/2$  is shown for (a) GBs=0 Hz and (b) GB=15 kHz cases. In the case of 15 kHz GB, the FC-F-OFDM achieves the synchronous UL CP-OFDM performance. Increasing the GB from this does not considerably improve the performance of synchronous CP-OFDM or asynchronous FC-F-OFDM, as it only reduces the differences between the waveform candidates.

#### G. Case 4: Mixed numerology UL link performance

In Fig. 14, the performance of different waveform candidates is shown for *Case 4* mixed numerology UL scenario in TD-LC 1000 ns channel with MCS 64-QAM,  $R = 1/2$  for the desired signal. The results are very similar to *Case 3* shown in Fig. 13. The CP-OFDM reference in synchronous UL is the one that was used in *Case 3* results to provide a realistic lower bound for the BLER performance. The link performance is given (a) without a GB and (b) with GB=15 kHz. In both

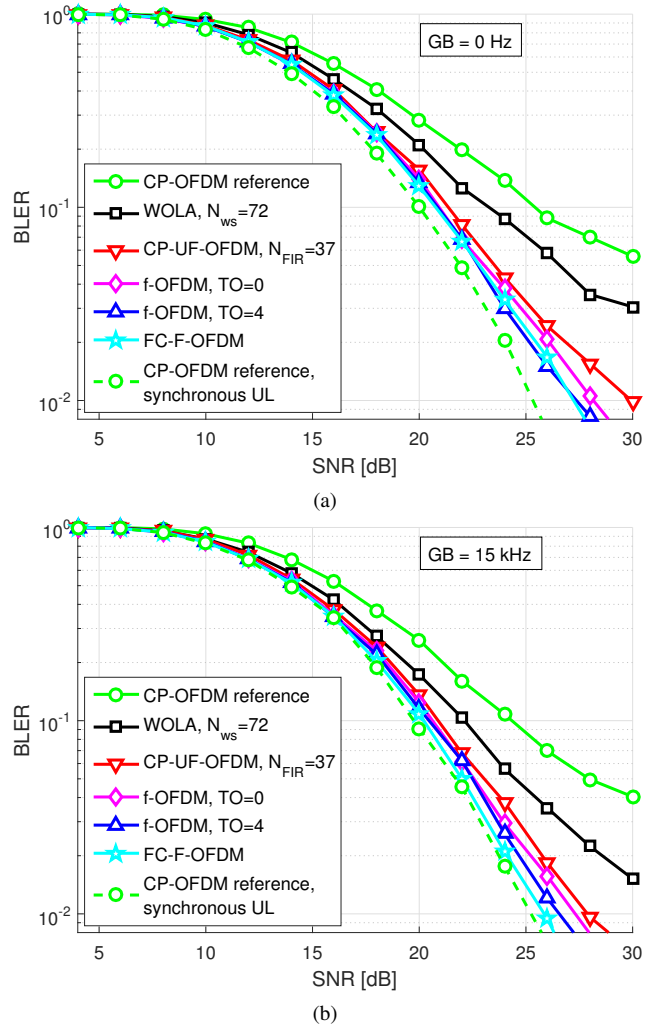


Fig. 13: Performance comparison for *Case 3* asynchronous UL scenario in TD-LC 1000 ns channel. The relative performance of different waveforms with (a) GB=0 Hz and (b) GB=15 kHz are shown.

cases, the given FC parameterization provides the best link performance. With GBs=15 kHz the FC-F-OFDM is able to achieve the synchronous UL CP-OFDM reference while the other waveform candidates lose approximately 2 dB at BLER target of 10%.

#### H. FC Filtered DFT-spread-OFDM

In [33], it was agreed that DFT-spread-OFDM is supported in UL in coverage limited scenarios. Therefore, in addition to spectral confinement, the maximum achievable PA output power is of great importance. In Fig. 15, PSDs and maximum PA output powers are shown for FC filtered DFT-spread-OFDM signal, assuming a 1 PRB allocation within a carrier of 50 PRBs. The transmitted signal is using MCS QPSK,  $R = 1/2$ , and the PA maximum output power is searched by brute force simulations where the minimum input backoff is searched with 0.1 dB step while fulfilling the in-band emission mask, OOBEM, and EVM requirements. In [39], the given EVM requirement for QPSK modulation is 17.5%. Here, EVM target of 12% was used for PA induced EVM. This threshold was selected to leave sufficient headroom for other TX imperfections, e.g., I/Q imbalance, phase noise, etc.

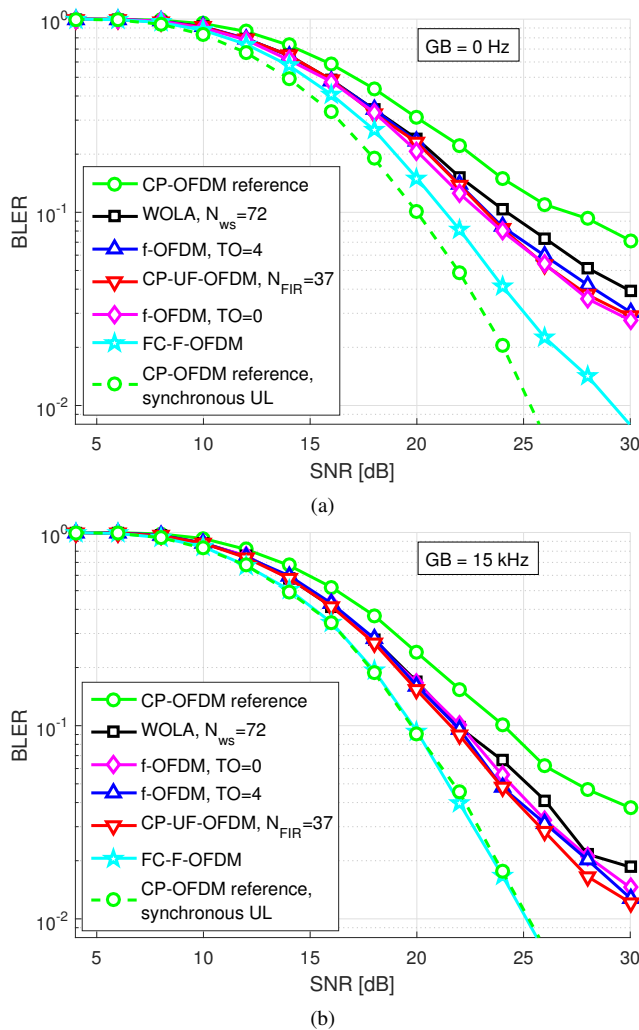


Fig. 14: Performance comparison for *Case 4* mixed numerology UL scenario in TDL-C 1000 ns channel. The relative performance of different waveforms with (a) GB=0 Hz and (b) GB=15 kHz are shown.

In Fig. 15 (a) different TBWs are compared with overlap factor  $\lambda = 1/2$  and  $\lambda = 1/4$ . The first observation is that the actual parameterization of the FC filtered DFT-s-OFDM has relatively small effect on the maximum PA output power and on the overall frequency response after the polynomial PA model. In the magnified subfigure the detailed differences between different TBWs are visible. The selection of larger TBW will affect SBLR over the neighboring PRB, but otherwise the performance is dictated by the PA induced spectral spreading. The observation that the lower overlap factor provides similar PA output powers and spectral containment allows to consider the overlap ratio  $\lambda = 1/4$  for UE to reduce the UE implementation complexity at least in coverage limited scenarios.

Furthermore, from Fig. 15, it is clear that as we push to increase the bandwidth efficiency by increasing the number of PRBs allocated in a certain channel, it is necessary to limit the maximum allowed PA output power in the edge-most PRBs. This is due to the significant spreading of the signal with small power backoffs, which would cause the presented examples to violate the LTE OOBEM if maximum allocation size would be 54 or 55 PRBs. Therefore, it is most likely that the higher bandwidth efficiency is first applied to DL, where

more linear PAs with efficient linearization and crest factor reduction algorithms are applied. As the UE PA technology evolves to support higher MCS for UL, the improved linearity will also allow larger bandwidth efficiency with the given coverage targets. Alternatively, only UEs using a high MCS could be scheduled to channel edges to fulfill the OOBEM. In this case, the passband MSE of the used subband filtering scheme is critical not to limit the set of usable MCSs.

In Fig. 15 (b) the performance of FC filtered DFT-spread-OFDM with 2 bin TBW is compared against a reference channel filtered DFT-s-OFDM and other subband constrained DFT-s-OFDM candidates. In current LTE UEs, channel filtering or windowing is required to achieve the OOBEM. From this example, a clear benefit of subband filtering on the in-band spectral containment is observed with respect to the channel filtered case. All of the waveform candidates provide very similar performance, but the magnified subfigure shows that the used FC filtered DFT-s-OFDM has the lowest leakage power nearby the allocation edge. In general, the maximum PA output power is approximately equal with all different subband processed signals allowing similar coverage as with channel filtering.

### I. Complexity vs. Performance Comparison

A basic computational complexity metric, the number of multiplications per QAM symbol, is shown in Table III for different subband configurations with FC-FB and time-domain filtering alternatives. The FC-FB complexity evaluation is based on the principles explained in [8]. With 50% overlap, the multiplication rates are 2.4–5.4 times the multiplication rates of a basic CP-OFDM transmitter or receiver, depending on the PRB configuration. Reducing the overlap factor from 50% to 25% reduces the multiplication rate by about 30%.

Effective time-domain implementation of an F-OFDM transmitter includes the steps listed below.

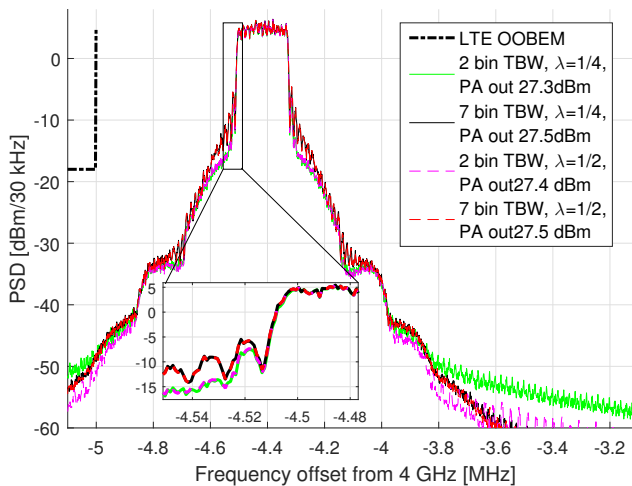
- 1) Length  $L$  IFFT taking  $(L(\log_2(L) - 3) + 4)/N_{\text{SYMB}}$  multiplications per symbol using the split-radix algorithm.  $N_{\text{SYMB}}$  is the number of QAM symbols per OFDM symbol in the subband.
- 2) Inserting CP
- 3) Interpolating lowpass filter with filter length of approximately  $N_{\text{FIR}}L/N$ , where  $N_{\text{FIR}}$  is the required length at the output sampling rate of 15.36 MHz. This is because FIR filter order is inversely proportional to the relative transition bandwidth. Making use of coefficient symmetry and noting that two real filters are needed (for in-phase and quadrature components), the multiplication rate becomes:  $N_{\text{FIR}}L(L + L_{\text{CP}})/(NN_{\text{SYMB}})$ .
- 4) Mixing at the output sampling rate taking  $4(N + L_{\text{CP}}N/L)/N_{\text{SYMB}}$  multiplications per symbol.

When the transmitted signal is composed of multiple subbands, the subbands are processed independently of each other, and in case of equal subband widths, the overall multiplication rate (per symbol) is equal to that of the single subband case.

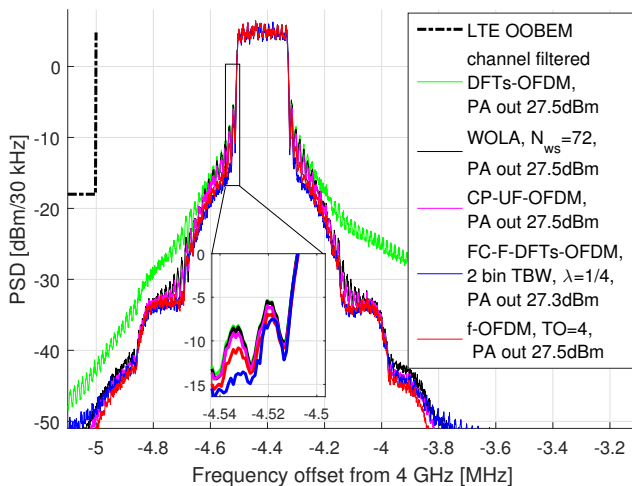
It can be concluded that time-domain implementation is effective in case of single or few narrow subbands, but for high number of subbands, or wide subbands, the FC-F-OFDM

TABLE III: FC based RX or TX complexity for different subband configurations with overlap factors of  $\lambda = 1/4$  and  $\lambda = 1/2$  in comparison with time-domain subband filtering approaches.

| No. active subcarriers | FC-F-OFDM                |                          |                             | CP-UF-OFDM, $N_{\text{FIR}} = 73$ | f-OFDM, $N_{\text{FIR}} = 512$ |
|------------------------|--------------------------|--------------------------|-----------------------------|-----------------------------------|--------------------------------|
|                        | Overlap factor $\lambda$ | Complexity (muls/symbol) | Complexity relative to OFDM | Complexity (muls/symbol)          | Complexity (muls/symbol)       |
| 1 PRB                  | 1/2                      | 1441.83                  | $\times 2.41$               | 512                               | 1139                           |
|                        | 1/4                      | 979.83                   | $\times 1.64$               |                                   |                                |
| 4 PRBs                 | 1/2                      | 360.46                   | $\times 2.41$               | 128                               | 285                            |
|                        | 1/4                      | 244.96                   | $\times 1.64$               |                                   |                                |
| 50 PRBs                | 1/2                      | 64.11                    | $\times 5.36$               | 133                               | 935                            |
|                        | 1/4                      | 46.89                    | $\times 3.92$               |                                   |                                |
| 12 $\times$ 4 PRBs     | 1/2                      | 61.51                    | $\times 4.94$               | 128                               | 285                            |
|                        | 1/4                      | 44.75                    | $\times 3.59$               |                                   |                                |



(a)



(b)

Fig. 15: PSDs and maximum PA output powers for 1 PRB transmission with (a) FC filtered DFT-spread-OFDM signal and (b) channel filtered and subband-filtered or windowed DFT-s-OFDM signals.

scheme is clearly more effective in terms of multiplication rate. Notably, FC-F-OFDM can provide very good spectrum localization with low complexity compared with corresponding time-domain realizations of F-OFDM. Furthermore, the proposed approach facilitates direct optimization of the frequency-domain window coefficients. Also high flexibility is achieved by a very small number of filter coefficients, determined by the transition bandwidth. In practice, it may be useful to have a few different sets of coefficients for different cases, e.g., wider transition band for the outer edges of the channel to achieve high OOB attenuation. Different transition band weight masks can also be combined in asymmetric manner. We have also seen that FC-F-OFDM gives in many cases the best, and practically always at least equally good EVM and in-band emission performance among the F-OFDM schemes.

On the other hand, the WOLA scheme needs only minor increase in complexity compared to the basic CP-OFDM and it has very good EVM performance. However, WOLA parametrization compatible with tentative 5G-NR numerology provides only limited improvement in the spectrum localization, and it is probably not sufficient for all intended 5G scenarios. Also enhanced time-domain windowing schemes are available in the literature. The edge windowing idea was originally proposed in [32] and later in [40] for 5G. The main benefit of this approach is that subcarriers in the center of a subband enjoy from almost full effective CP length, while long window transitions are applied only for subcarriers close to the subband edges. In our simulation examples, the overall CP-OFDM symbol duration is not extended in the WOLA case, which leads to degraded performance with high delay spread channels, like TDL-C 1000 ns. By using edge windowing, the multipath delay-spread tolerance could be improved for the center subcarriers in case of wide subcarrier allocations, while the spectral containment results would experience relatively small degradation compared to the presented results. On the other hand, implementation complexity would be significantly increased, and edge windowing would also add some complexity to the resource allocation function [32].

## V. CONCLUSIONS

We have proposed a straightforward and efficient technique for designing and optimizing the FC-F-OFDM based physical



layer waveform processing in 5G mobile cellular radio networks, building on the concept of subband filtering on top of the baseline CP-OFDM waveform. For given transition bandwidth, different tradeoffs between the passband EVM performance and in-band emissions, in terms of the subband leakage ratio, can be obtained in a flexible manner. The current optimization framework uses the minimum stopband attenuation value as an optimization constraint, allowing to control the band-limitation characteristics of the subband signals in an efficient manner. In general, good match was demonstrated between the simplified system model used in the optimization and actual simulated radio link performance in tentative 5G-NR test scenarios, incorporating different levels of asynchronism between UL users, different numerologies for different subbands, as well as different radio channel propagation characteristics at sub-6 GHz bands.

The obtained results show that the optimization based design of FC-F-OFDM physical layer achieves the EVM requirements and often significantly exceeds the SBLR and the overall radio link performance of the existing time-domain filtering based realizations of F-OFDM or windowing based CP-OFDM. In general, time-domain filtering based schemes are computationally effective for cases with single narrow filtering subband (e.g. 1–4 PRBs), so they could be particularly useful for low-rate user devices. In full-band cases (e.g. 50 PRBs in a 10 MHz LTE channel), however, both with single or multiple subbands, the proposed FC-F-OFDM has significantly lower complexity. It is able to provide effective filtering for the whole carrier with narrow transition bands, allowing, as a concrete example, to increase the number of PRBs from 50 to 55 in case of a 10 MHz carrier. Furthermore, FC-F-OFDM has the flexibility to construct arbitrary subband configurations, as groups of PRBs, with minimal coefficient storage requirements, which provides substantial implementation benefits. Our future work will focus on revisiting the formulation of the optimization framework for FC-F-OFDM, using an explicit constraint on the adjacent subband SBLR, instead of the currently used minimum stopband attenuation requirement.

## REFERENCES

- [1] J. Yli-Kaakinen, T. Levanen, M. Renfors, and M. Valkama, "Optimized fast convolution based filtered-OFDM processing for 5g," submitted to *European Conf. on Networks and Communications (EUCNC 2017)*, Oulu, Finland, Jun. 2017.
- [2] A. Toskala and H. Holma, Eds., *LTE for UMTS – OFDMA and SC-FDMA Based Radio Access*. Wiley, 2009.
- [3] G. Wunder, P. Jung, M. Kasparick, T. Wild, F. Schaich, Y. Chen, S. Brink, I. Gaspar, N. Michailow, A. Festag, L. Mendes, N. Cassiau, D. Ktenas, M. Dryjanski, S. Pietrzyk, B. Eged, P. Vago, and F. Wiedmann, "5GNOW: Non-orthogonal, asynchronous waveforms for future mobile applications," *IEEE Commun. Mag.*, vol. 52, no. 2, pp. 97–105, Feb. 2014.
- [4] P. Banelli, S. Buzzi, G. Colavolpe, A. Modenini, F. Rusek, and A. Ugolini, "Modulation Formats and Waveforms for 5G Networks: Who Will Be the Heir of OFDM?: An overview of alternative modulation schemes for improved spectral efficiency," *IEEE Signal Processing Magazine*, vol. 31, no. 6, pp. 80–93, Nov 2014.
- [5] R. Ahmed, T. Wild, and F. Schaich, "Coexistence of UF-OFDM and CP-OFDM," in *IEEE 83rd Vehicular Technology Conference (VTC Spring)*, May 2016, pp. 1–5.
- [6] X. Zhang, M. Jia, L. Chen, J. Ma, and J. Qiu, "Filtered-OFDM – Enabler for flexible waveform in the 5th generation cellular networks," in *2015 IEEE Global Communications Conference (GLOBECOM)*, Dec. 2015, pp. 1–6.
- [7] J. Li, E. Bala, and R. Yang, "Resource block filtered-OFDM for future spectrally agile and power efficient systems," *Physical Communication*, vol. 14, pp. 36–55, Jun. 2014.
- [8] M. Renfors, J. Yli-Kaakinen, T. Levanen, M. Valkama, T. Ihalainen, and J. Vihriälä, "Efficient Fast-Convolution Implementation of Filtered CP-OFDM Waveform Processing for 5G," in *2015 IEEE Globecom Workshops*, San Diego, CA, USA, Dec. 2015.
- [9] M. Renfors, J. Yli-Kaakinen, T. Levanen, and M. Valkama, "Fast-convolution filtered OFDM waveforms with adjustable CP length," in *Proc. Global Conference on Signal and Information Processing (GlobalSIP)*, Greater Washington, D.C., USA, in press.
- [10] Nokia, "R1-165014, Subband-wise filtered OFDM for New Radio below 6 GHz," 2016, 3GPP TSG-RAN WG1 Meeting #85.
- [11] Qualcomm, "R1-162199, Waveform Candidates," 2016, 3GPP TSG-RAN WG1 Meeting #84b.
- [12] Nokia, "R1-167246, On independent design of Tx and Rx units for NR," 2016, 3GPP TSG-RAN WG1 Meeting #86.
- [13] "R1-167963, Way forward on waveform," 2016, 3GPP TSG-RAN WG1 Meeting #86.
- [14] 3GPP TR 38.802 V1.0.0, "Study on New Radio (NR) Access Technology Physical Layer Aspects (Release 14)," Nov. 2016.
- [15] J. Yli-Kaakinen and M. Renfors, "Optimized reconfigurable fast convolution based transmultiplexers for cognitive radio," submitted to *IEEE Trans. Circuits Syst II*, Oct. 2016.
- [16] L. R. Rabiner and B. Gold, *Theory and Application of Digital Signal Processing*. Englewood Cliffs, NJ: Prentice-Hall, 1975.
- [17] M. Borgerding, "Turning overlap-save into a multiband mixing, down-sampling filter bank," *IEEE Signal Processing Mag.*, pp. 158–162, Mar 2006.
- [18] M.-L. Boucheret, I. Mortensen, and H. Favaro, "Fast convolution filter banks for satellite payloads with on-board processing," *IEEE J. Select. Areas Commun.*, vol. 17, no. 2, pp. 238–248, Feb. 1999.
- [19] C. Zhang and Z. Wang, "A fast frequency domain filter bank realization algorithm," in *Proc. Int. Conf. Signal Processing*, vol. 1, Beijing, China, Aug. 21–25 2000, pp. 130–132.
- [20] L. Pucker, "Channelization techniques for software defined radio," in *Proc. Software Defined Radio Technical Conference (SDR'03)*, Orlando, FL, USA, Nov. 18–19 2003.
- [21] M. Renfors, J. Yli-Kaakinen, and F. Harris, "Analysis and design of efficient and flexible fast-convolution based multirate filter banks," *IEEE Trans. Signal Processing*, vol. 62, no. 15, pp. 3768–3783, Aug. 2014.
- [22] K. Shao, J. Alvava, J. Yli-Kaakinen, and M. Renfors, "Fast-convolution implementation of filter bank multicarrier waveform processing," in *IEEE Int. Symp. on Circuits and Systems (ISCAS 2015)*, Lisbon, Portugal, May 24–27 2015, pp. 978–981.
- [23] M. Renfors and J. Yli-Kaakinen, "Flexible fast-convolution implementation of single-carrier waveform processing," in *IEEE Int. Conf. on Communications Workshops, ICCW 2015*, London, UK, Jun. 8–12 2015, pp. 1243–1248.
- [24] J. Yli-Kaakinen and M. Renfors, "Optimization of flexible filter banks based on fast convolution," *Journal of Signal Processing Systems*, vol. 85, no. 1, pp. 101–111, Aug. 2016.
- [25] A. Daher, E.-H. Baghious, G. Burel, and E. Radoi, "Overlap-save and overlap-add filters: Optimal design and comparison," *IEEE Trans. Signal Processing*, vol. 58, no. 6, pp. 3066–3075, Jun. 2010.
- [26] H. Lin and P. Siohan, "Multi-carrier modulation analysis and WCP-COQAM proposal," *EURASIP Journal on Advances in Signal Processing*, vol. 2014, no. 1, pp. 1–19, 2014. [Online]. Available: <http://dx.doi.org/10.1186/1687-6180-2014-79>
- [27] M. Renfors and J. Yli-Kaakinen, "Timing offset compensation in fast-convolution filter bank based waveform processing," in *Proc. Int. Symp. Wireless Communication Systems (ISWCS 2013)*, Ilmenau, Germany, Aug. 2013.
- [28] J. Yli-Kaakinen and M. Renfors, "Multi-mode filter bank solution for broadband PMR coexistence with TETRA," in *Proc. European Conf. on Networks and Communications*, Bologna, Italy, Jun. 2014.
- [29] M. Renfors and J. Yli-Kaakinen, "Channel equalization in fast-convolution filter bank based receivers for professional mobile radio," in *Proc. European Wireless*, Barcelona, Spain, May 14–16 2014.
- [30] Qualcomm, "5G Waveform & Multiple Access Techniques," 2015, online: [www.qualcomm.com/media/documents/files/5g-waveform-multiple-access-techniques.pdf](http://www.qualcomm.com/media/documents/files/5g-waveform-multiple-access-techniques.pdf), last accessed 3 June 2016.
- [31] 3GPP TR 25.892 V6.0.0, "Feasibility Study for Orthogonal Frequency Division Multiplexing (OFDM) for UTRAN enhancement (Release 6)," Jun. 2004.

- [32] A. Sahin and H. Arslan, "The impact of scheduling on edge windowing," in *2011 IEEE Global Telecommunications Conference - GLOBECOM 2011*, Dec 2011, pp. 1–5.
- [33] "R1-1610485, WF on waveform for NR uplink," 2016, 3GPP TSG-RAN WG1 Meeting #86-Bis.
- [34] 3GPP TS 36.104 V13.3.0, "Evolved Universal Terrestrial Radio Access (E-UTRA); Base Station (BS) Radio Transmission and Reception (Release 13)," Mar. 2016.
- [35] 3GPP TR 38.900 V14.0.0, "Study on channel model for frequency spectrum above 6 GHz," Jun. 2016.
- [36] Nokia, "R1-167297, [85-18] PA assumptions for NR; email discussion summary," 2016, 3GPP TSG-RAN WG1#86.
- [37] T. Säynäjäkangas, "R1-166004, response LS on realistic power amplifier model for NR waveform evaluation," 2016, 3GPP TSG-RAN WG1 Meeting #85.
- [38] 3GPP TS 36.300 V13.3.0, "Evolved Universal Terrestrial Radio Access (E-UTRA) and Evolved Universal Terrestrial Radio Access Network (E-UTRAN); Overall Description; Stage 2 (Release 13)," Mar. 2016.
- [39] 3GPP TS 36.101 V13.3.0, "Evolved Universal Terrestrial Radio Access (E-UTRA); User Equipment (UE) Radio Transmission and Reception (Release 13)," Mar. 2016.
- [40] Samsung, "R1-166746, Discussion on multi-window OFDM for NR waveform," 2016, 3GPP TSG-RAN WG1 Meeting #86.



**Juha Yli-Kaakinen** received the degree of Diploma Engineer in electrical engineering and Doctor of Technology (with honors) from the Tampere University of Technology (TUT), Tampere, Finland, in 1998 and 2002, respectively.

Since 1995, he has held various research positions at TUT. His research interests are in digital signal processing, especially in digital filter and filter bank optimization for communication systems and VLSI implementations.



**Toni Levanen** received the M.Sc. (with honours) and D.Sc. degrees in Digital communications from Tampere University of Technology (TUT), Finland, in 2007 and 2014, respectively. He is currently a researcher with the Laboratory of Electronics and Communications Engineering, TUT. In addition to his contributions in academic research, he has worked in industry on wide variety of development and research projects for communications systems. His current research interests include physical layer design for 5G NR, traffic and interference modeling

in 5G small cells and millimeter-wave communications, and high-mobility support in ultra-dense small cell networks.



**Sami Valkonen** received his B.Sc. in 2015 from Tampere University of Technology. He is currently pursuing his M.Sc. degree on wireless mobile communications with research interest in time-domain windowed and subband-filtered CP-OFDM waveforms for 5G new radio.



**Kari Pajukoski** received his B.S.E.E. degree from the Oulu University of Applied Sciences in 1992. He is a Fellow with the Nokia Bell Labs. He has a broad experience from cellular standardization, link and system simulation, and algorithm development for products. He has more than 100 issued US patents, from which more than 50 have been declared "standards essential patents". He is author or co-author of more than 300 standards contributions and 30 publications, including conference proceedings, journal contributions, and book chapters.



**Juho Pirskanen** received his M.Sc. in Electrical Engineering from Tampere University of Technology in 2000. Since then, he has worked in several different positions on wireless radio research, technology development, and standardization at Nokia Bell Labs, Nokia Networks, Nokia, Renesas Mobile and Broadcom Corporation. He has participated actively standardization of 3G, HSPA, LTE, 5G and WLAN technologies by leading the standardization delegation in 3GPP and in IEEE802.11. His latest research activities include 3GPP 5G NR physical

layer, control layer, and network design.



**Markku Renfors** (S'77–M'82–SM'90–F'08) received the D.Tech. degree from Tampere University of Technology (TUT), Tampere, Finland, in 1982. Since 1992, he has been a Professor with the Department of Electronics and Communications Engineering, TUT, where he was the Head from 1992 to 2010. His research interests include filter bank based multicarrier systems and signal processing algorithms for flexible communications receivers and transmitters. Dr. Renfors was a corecipient of the Guillemin Cauer Award (together with T. Saramäki) from the IEEE Circuits and Systems Society in 1987.



**Mikko Valkama** was born in Pirkkala, Finland, on November 27, 1975. He received the M.Sc. and Ph.D. Degrees (both with honours) in electrical engineering (EE) from Tampere University of Technology (TUT), Finland, in 2000 and 2001, respectively. In 2002, he received the Best Ph.D. Thesis -award by the Finnish Academy of Science and Letters for his dissertation entitled "Advanced I/Q signal processing for wideband receivers: Models and algorithms". In 2003, he was working as a visiting researcher with the Communications Systems and Signal Processing

Institute at SDSU, San Diego, CA. Currently, he is a Full Professor and Department Vice-Head at the Department of Electronics and Communications Engineering at TUT, Finland. He has been involved in organizing conferences, like the IEEE SPAWC'07 (Publications Chair) held in Helsinki, Finland. His general research interests include communications signal processing, estimation and detection techniques, signal processing algorithms for software defined flexible radios, cognitive radio, full-duplex radio, radio localization, 5G mobile cellular radio, digital transmission techniques such as different variants of multicarrier modulation methods and OFDM, and radio resource management for ad-hoc and mobile networks.